8-11-2007

Determination of best practice guidelines for performing large eddy simulation of flows in configurations of engineering interest

Adetokunbo Adelana Adedoyin

Follow this and additional works at: https://scholarsjunction.msstate.edu/td

DETERMINATION OF BEST PRACTICE GUIDELINES FOR PERFORMING

LARGE EDDY SIMULATION OF FLOWS IN CONFIGURATIONS OF

ENGINEERING INTEREST

By

Adetokunbo Adelana Adedoyin

A Thesis
Submitted to the Faculty of
Mississippi State University
in Partial Fulfillment of the Requirements
for the Degree of Master of Science
in Mechanical Engineering
in the Department of Mechanical Engineering

Mississippi State, Mississippi

August 2007

DETERMINATION OF BEST PRACTICE GUIDELINES FOR PERFORMING

LARGE EDDY SIMULATION OF FLOWS IN CONFIGURATIONS OF

ENGINEERING INTEREST

By

Adetokunbo Adelana Adedoyin

Approved:

_____
Dibbon K. Walters
Assistant Professor of Mechanical
Engineering
(Major Professor)

_____
Eric Blades
Assistant Professor of Computational
Engineering
(Committee Member)

_____
Rogelio Luck
Associate Professor of Mechanical
Engineering
(Committee Member)

_____
Steve R. Daniewicz
Professor of Mechanical
Engineering,
and Graduate Coordinator, Department
of Mechanical Engineering

_____
W. Glenn Steele
Interim Dean
of the Bagley College of Engineering

Name: Adetokunbo Adelana Adedoyin

Date of Degree: August 11, 2007

Institution: Mississippi State University

Major Field: Mechanical Engineering

Major Professor: Dr. Dibbon K. Walters

Title of Study: DETERMINATION OF BEST PRACTICE GUIDELINES FOR PER-
FORMING LARGE EDDY SIMULATION OF FLOWS IN CONFIG-
URATIONS OF ENGINEERING INTEREST

Pages in Study: 93

Candidate for Degree of Master of Science

Large eddy simulation (LES) suffers from two primary sources of error: the numerical
discretization scheme and the subgrid stress model (SGS). An attempt has been made
to determine optimum combinations of SGS models and numerical schemes for use in
performing practical LES for engineering-relevant problems.

A formal quantification of numerical error present in finite-volume/finite-difference
simulations was conducted. The effect of this error was explicitly added to a pseudospec-
tral LES solver, and the modified pseudospectral solver was used to compute LES of de-
caying turbulence. In this way SGS modeling error and numerical error could be separately
assessed.

Verification of results was carried out using a commercially available finite-volume
solver ($FLUENT^{®}$). Results showed that some combinations of SGS model and dis-
cretization scheme are more suitable for performing LES than others. Favorable combi-

nations from the above findings were tested for an axisymmetric jet at Mach number 0.2.

Results indicate good agreement with prior findings.

DEDICATION

To all involved in the advancement of knowledge in turbulent flow.

ACKNOWLEDGMENTS

TABLE OF CONTENTS

LIST OF TABLES

LIST OF FIGURES

LIST OF SYMBOLS, ABBREVIATIONS, AND NOMENCLATURE

DNS Direct numerical simulation

LES Large eddy simulation

SGS Subgrid stress

ℓ A variable representing the integral (i.e. large) scales of motion

η A variable representing the inertia (i.e. small) scales of motion

Δt A variable representing time stepsize

Δx A variable representing mesh spacing

ν A variable representing viscosity

$G(x, \acute{x})$ A spatial filter function

δ Numerical error operator

CD Central difference numerical scheme

Q QUICK numerical scheme

2U Second order upwind numerical scheme

1U First order upwind numerical scheme

BCD Bounded central difference numerical scheme

SM Smagorinsky subgrid stress model

DSM Dynamic smagorinsky subgrid stress model

MILES Monotonically integrated subgrid stress modeling approach

MSM Multiscale subgrid stress model

Re Reynolds number of a flow

FHW Data collected using a flying hot wire

SHW Data collected using a stationary hot wire

LDA Data collected using a laser dopper anemometer

CHAPTER 1

INTRODUCTION

1.1 Background

Around the early nineteenth century the common approach to solving fluid dynamics problems, as adopted by Prandtl and others, was the pencil-and-paper method. Today, this method is no longer sufficient. The steady rise in computer processing power has fostered the development of a wide range of investigations in fluid dynamics. New tools are constantly being developed and have led to the emergence of a modern approach to tackling fluid dynamics problems, computational fluid dynamics (CFD). With CFD, a wide range of engineering problems can be resolved numerically. As most flows of engineering importance are turbulent, large eddy simulation (LES) is becoming a common approach to tackling turbulent flow fields. Reasons for this can be attributed to the computational and theoretical advantages of LES over other methods.

Direct numerical simulation (DNS) remains computationally infeasible for most flows of engineering interest. Conceptually, DNS of the Navier-Stokes (NS) equations is the simplest approach. It consists of numerically representing the instantaneous NS equations, resolving all scales of motion, and proceeding in time for a given set of initial and boundary

conditions. For DNS, the level of description of a single realization of the flow remains unmatched. However, the implications of such a high fidelity solution are enormous.

Performing DNS on a simple cubic domain Ω with sides of length L involves a resolution of scales of motion ranging from the integral (ℓ) to the Kolmogorov microscale (η). The Kolmogorov microscale approximates as $\eta = Re^{-3/4}\ell$, where Re represents the Reynolds number. Numerically, a prescribed grid size such as $\Delta x \approx \eta = Re^{-3/4}\ell$, is required to capture the smallest scales of motion. Consequently, for a three dimensional simulation the number of data points required every iteration approximates as $N_i \approx (L/\Delta x)^3 \approx (L/\ell)^3 Re^{9/4}$. Further, it can be determined that the minimum time step sufficient to simulate a particle movement within one grid cell is $\Delta t \approx \Delta x/u$ or $\Delta t \approx \eta/u$. For a total iteration time T, the number of time steps required is $N_j \approx T/\Delta t \approx Tu/\eta = Tu/(Re^{-3/4}\ell)$. Total computational time therefore scales as $CPU_t \approx N_i N_j \approx (L/\ell)^3 (uT/\ell) Re^3$. From this, it is apparent that the required CPU time is strictly dependent on powers of Reynolds number. Therefore, for flows of practical engineering interest (which typically have large Reynolds numbers) DNS remains a prohibitively expensive tool for computing turbulent dynamics.

A seemingly suitable alternative is computing a turbulent flow field using the Reynolds-averaged Navier-Stokes (RANS) equations. RANS involves projecting a turbulent flow field into its mean ensemble averaged or time averaged component. In this case, the unknowns are the Reynolds stresses, modeled either by the turbulent viscosity hypothesis or the Reynolds-stress transport equations. As a result of its computational efficiency, the RANS technique is widely used. However, disadvantages of RANS include poor accuracy

due to modeling of the inherent empiricism required for Reynolds stresses. Also details of the flow field are lost due to the averaging process.

Large eddy simulation (LES), whereby the large energy containing eddies of a turbulent flowfield are resolved, is quickly becoming a feasible option for understanding the dynamics of turbulent flow. LES has grown in popularity with researchers and scientist over the past three decades. It is less expensive computationally than DNS. In addition, the results are usually of an acceptable degree of accuracy for engineering flows. Favorable theoretical bases that support LES include the observation that the dynamics of turbulent flow is dominated by large scale motions. This permits the assumption that large eddies determine the direction and amount of momentum and energy transfer. For simplicity, LES follows the assumption that kinetic energy transfer is from large to small scales of motion. LES involves resolving the large eddies and modeling the smaller ones by an eddy dissipation parameter. Another theoretical support for LES follows from the observation that small scale eddies appear nearly isotropic in nature, implying that the small scales are less cumbersome to model than the entire range of turbulent motion, as required in RANS.

The growing adoption of LES for engineering problems has led to a substantial development in the literature on its application to turbulent flow. Most research in LES has been focused in two directions. The first direction of research concerns itself with the more fundamental issues in LES; modeling of the residual (i.e. small-scale) motion and development of accurate numerical schemes for structured and unstructured grids. Testing is usually performed for simple canonical flows. These kind of studies usually focus on assessment of a higher order scheme or development of an accurate subgrid stress model.

3

The second direction of research is usually geared towards validating results from performing large eddy simulations on flows of practical engineering significance. Validation usually proceeds by comparing results to experimental data and/or a RANS simulation. The focus is usually on obtaining good results using an available general-purpose CFD solver.

This research effort represents a bridge between these two types of study. This work proceeds by presenting a detailed analysis of error sources present in large eddy simulation using a general-purpose CFD solver. The primary sources of error in LES are the prescribed numerical and physical parameters: the subgrid stress model and the numerical discretization scheme. For finite-volume/finite-difference simulations, these error sources are distinct though inseparable and act together in a nonlinear manner. Therefore, there is need to be able to assess the coupled interactions and further to determine optimum combinations of closure model and discretization schemes for use in performing LES in complex engineering environments. Specific to the study presented here is LES of high-Reynolds-number decaying isotropic turbulence implemented using second order accurate schemes and common subgrid stress models. The simulations were designed following the experimental test case of Kang et al. [15]. Simulations were first performed using a pseudospectral solver previously validated for prediction of isotropic decaying turbulence [3]. With the pseudospectral method, subgrid stress modeling error can be isolated from discretization error, which is not possible for finite-difference/finite-volume LES. Following this, numerical error present in finite-volume/finite-difference large eddy simulations was explicitly incorporated into the pseudospectral LES solver. Verification of the pseudospec-

tral results was carried out using a commercially available finite-volume/finite-difference solver (FLUENT®). From there, suitable combinations of subgrid stress model and numerical discretization scheme were determined. Several combinations were then tested for large eddy simulation of a high-Reynolds-number, momentum conserving, axisymmetric turbulent jet at Mach number 0.2, and compared to the experimental data of Hussein et al. [14].

CHAPTER 2

LITERATURE REVIEW

2.1 Literature Review

The concept and practical implementation of large eddy simulation has developed due to the need to be able to compute and understand the dynamics of three dimensional unsteady turbulent motions without resorting to computationally expensive DNS [8, 24]. For most engineering applications, large eddies are primarily responsible for mass, momentum, and energy transport. The success of large eddy simulation as a tool lies in the fact that most quantities of interest and rate-controlling processes are primarily controlled by the resolved large scales of motion [25]. Conceptually, large eddy simulation constitutes resolving the large energy containing eddies and modeling the small (unresolved) ones. The mathematical implication of this is the application of a low-pass filter to the Navier -Stokes equations [13]. In this way, the dominant flow structures can be exclusively accounted for. The filtering operation is expressed mathematically as:

$$\bar{f}_i(x) = \int G(x, \acute{x}) f_i(\acute{x}) d\acute{x} \tag{2.1}$$

As shown in 2.1, the resulting field is a convolution of the velocity field with a filter function, $G(x, \acute{x})$, that filters out higher wavenumber structures. Applying the filter function, $G(x, \acute{x})$, to the governing equation for an incompressible flow in divergence form gives:

$$\frac{\partial \bar{u}_j}{\partial x_j} = 0 \tag{2.2}$$

$$\frac{\partial \bar{u}_i}{\partial t} + \frac{\partial \bar{u}_i \bar{u}_j}{\partial x_j} = -\frac{\partial \bar{p}}{\partial x_i} + \frac{\partial}{\partial x_j}\left(\nu \frac{\partial \bar{u}_i}{\partial x_j}\right) - \frac{\partial \tau_{ij}}{\partial x_j} \tag{2.3}$$

$$\tau_{i,j} = \overline{u_i u_j} - \bar{u}_i \bar{u}_j \tag{2.4}$$

where 2.4 represents the subgrid stress tensor which must be modeled in order to close the equation set. The resulting equation is the filtered Navier-Stokes equation commonly solved using either finite-volume/finite-difference methods or spectral techniques. For finite-volume/finite-difference methods, the governing equations are solved in real (physical) space, while for spectral techniques the equation are transformed and resolved in wavenumber (spectral) space.

Considered here is homogeneous turbulence for which application of a sharp cutoff filter is possible in spectral space, i.e. all wavenumber modes less than a cutoff wavenumber are completely resolved, and all wavenumber modes greater than the cutoff wavenumber are completely unresolved. For simplicity, a filter to grid width ratio of unity is assumed. Traditionally, large eddy simulation filters are embedded implicitly though several explicit methods have also been developed [27]. Of concern here is finite-volume numerical methods, where a volume average corresponds to convolution of the velocity field with a box filter and sharp cutoff of all scales of motion beyond the cutoff wavenumber which is dictated by the grid size. The effect of volume averaging is a smooth filter in spectral space.

7

In that case, there is a subfilter component associated with all scales of motion including those larger than the grid size (i.e. resolved scales). Following [29], the filtered field is simulated here without consideration of a formal separation of scale. Therefore, the sub-grid stress tensor (2.4) in this work represents the total effect of the unresolved velocity field on the resolved part, as shown in Figure 2.1.
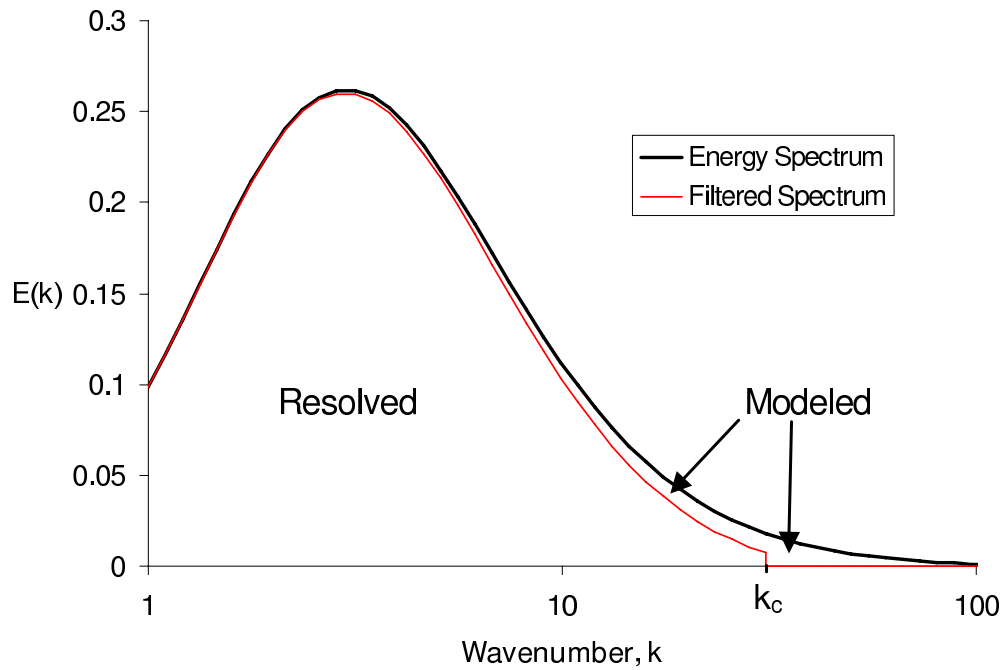

Figure 2.1

See appendix for details

Using finite-volume/finite-difference methods, numerical discretization error in large eddy simulation of turbulent flow is inherent. It can be categorized into two types: truncation and aliasing error. Truncation error is due to numerical evaluation of derivatives in 2.2

8

and 2.3. Aliasing error is as a result of numerically evaluating the nonlinear momentum convective term in equation 2.3.

$$\frac{\partial \left(\bar{u}_i \bar{u}_j \right)}{\partial x_j} \tag{2.5}$$

In spectral space, aliasing error is due to the interaction of coefficients of wavenumber modes outside the resolution subrange. Several spectral blocking methods have being prescribed for eradicating aliased modes [5]. Adopted here is the the $\frac{3}{2}$ rule, previously validated in [3] and explained in chapter three. Formal methods of error analysis, as those performed with linear partial differential equations (i.e Laplace equation), suffice to be insightful tools in constructing SGS models. However, they are incapable of accurately quantifying highly nonlinear turbulent fields [4].

Ghosal [12] pursued a rigorous approach to analyzing error present in large eddy simulation. He considered isotropic turbulence in a cubic domain, with periodic boundary conditions. His formulation of the flow equations adopted the divergence form of the nonlinear term (2.5). In his work, he proceeded by utilizing the joint-normal approximation to derive analytical expressions for the power spectra of errors present in simulating turbulent fields. In this way, he was able to create qualitative bounds on the magnitude of the numerical error. His results show that second order schemes are least desirable for turbulent simulations. Specifically, he mentions that finite-difference error appears to be much larger than the subgrid stress contribution for most wavenumbers. The goal of a subgrid stress model is to closely predict the influence of unresolved scales on resolved scales. According to Ghosal [12], the subgrid model will not function as intended if it is being masked out by numerical error. His findings also show that aliasing error is most dominant

for higher order schemes. His suggestion for performing turbulent simulations is to use a higher order scheme with a filter to grid width ratio of $\frac{\Delta_f}{\Delta_g} = 2$, for higher accuracy.

Ghosal's [12] technique is widely acknowledged in literature. It is often categorized as a static approach to error analysis. It sufficed to be an insightful tool, however, it does not address the time dependent nature of non-linear interactions between SGS force and numerical error. Park et al. [22] formulated a dynamic approach to error quantification in LES of decaying turbulence. In order to model temporal interactions, they derived a transport equation for the energy spectrum. Upon derivation, a quadruple nonlinear term appears on the right-hand-side, which they then closed by introducing the quasi-normal assumption (quasi-normal $\Rightarrow$ joint-normal hypothesis). Further, they add an eddy damping rate to the $E(\kappa)$ transport equation. They then apply "Markovianization" to the resulting equation to ensure positive definiteness. The resulting equation is a one-dimensional (1D) differential equation solvable using any accurate numerical method. This statistical theory is known as the "Eddy Damped Quasi-Normal Markovian" (EDQNM). With this, the energy spectrum of the Navier-Stokes equations can be simulated without performing the actual domain evolution and in that case it is denoted as EDQNM-DNS. Similarly, the energy spectrum of the LES equations can be simulated if an additional term is added onto the EDQNM equation accounting for subgrid activity. In defending a dynamic approach as opposed to a static error analysis technique, Park et al. [22], mention that the divergence form of the nonlinear term in the NS equation should not be used, (as used by Ghosal [12]), because it violates kinetic energy conservation [16]. Park et. al [22] further show that the resulting EDQNM-LES system predicts the actual NS-LES system to an accept-

able degree, at consecutively later time realizations. They proceed by pursuing a dynamic analysis of all error contributions including the viscous terms and the numerical error. Opposed to the conclusion of Ghosal [12], Park et al. [22] assert that the contribution of the SGS model to the LES solution is more pronounced than the truncation and aliasing error associated with a second order finite-differencing scheme. The results also show that numerical errors lead to dispersion of energy at intermediate wavemumbers while the contribution of the SGS model shows a significant removal of energy at all wavenumbers and a maximum at the cutoff-wavenumber (k_c). Park et al.'s [22] conclusions imply that useful LES can be performed using lower order schemes.

In a prior publication, Park et al. [23], investigated the suitability of central and upwind-biased schemes for performing LES of turbulent flow. They proceeded in their investigations by performing a static error analysis following [12] as well as performing simulations with an actual domain evolution. They also addressed the performance differences in implementing different forms of the nonlinear term. Their results show that for the static error analysis, finite-differencing error increased as well as aliasing error with an decrease in numerical dissipation. Contrary to this, their simulation results show that finite-differencing error decreased with an increase in numerical dissipation. In this way, aliasing error completely outweighs finite-difference error. From this they concluded that a static error analysis does not properly chacterize discretization influence and that a dy-

namic approach is necessary. The results from testing different forms of the nonlinear term showed that the skew symmetric form of the nonlinear term, (2.6),

$$\frac{1}{2}\left[\frac{\partial\left(\bar{u}_i\bar{u}_j\right)}{\partial x_j} + \frac{\bar{u}_j\partial\left(\bar{u}_i\right)}{\partial x_j}\right] \tag{2.6}$$

$$\frac{\bar{u}_j\partial\left(\bar{u}_i\right)}{\partial x_j} \tag{2.7}$$

yields better results compared to the divergent form 2.5 or the convective form 2.7. It minimizes the finite-difference and aliasing error relative to the other forms. In addition, Park et al. [23] discovered that there exist an optimum degree of upwinding that minimizes total discretization errors implying that a scheme that combines the effects of a central differencing and an upwind scheme will be most suitable for performing LES of decaying turbulence.

On the subtopic of the appropriate form for the nonlinear term, Fedioun et al. [9] propose a modified approach to error analysis in spectral space. They show that prior investigation on error analysis using dealiased spectral codes may lead to erroneous results. Further, they show that aliased pseudospectral results are equivalents of physical space calculations. They propose a modified-wavenumber approach to static error analysis in spectral space for use in physical space simulation. They performed simulations of decaying isotropic turbulence using second order and sixth order compact finite-differencing schemes combined with all forms of the non-linear term. They concluded that for lower (i.e. second) order schemes, truncation error is the dominant form of numerical error for all forms of the nonlinear term. These conclusions are critical, particularly because an important element in this study is numerical error (i.e. truncation error) generated from 2nd

order discretization schemes and their interactivity with SGS models in the pseudospectral simulations. Further, they demonstrated that the convective form 2.7 yield better results than other forms of the nonlinear term. It is important to note, however that general-purpose CFD solvers commonly adopt the divergence form, (2.5), of the nonlinear term in order to satisfy conservation properties.

2.1.1 Thesis statement

This paper extends the prior findings outlined above in order to perform error analysis on LES for use in physical space simulations. The investigation proceeded in two parts. A pseudospectral solver was used to compute LES of decaying isotropic turbulence on both 32^3 and 64^3 grid resolutions. In this way, the SGS modeling error can be isolated. Following this, a formal quantification of error present in finite-volume/finite-difference simulations was conducted. The effect of this error was then explicitly incorporated into the pseudospectral LES solver.

The solution set from this procedure creates a forum for understanding the interaction between SGS models and discretization schemes in large eddy modeling. Comparisons are made in terms of energy spectra corresponding to different downstream positions in the wind tunnel used in the experimental test case. Verification of results is then carried out using a commercially available finite-volume/finite-difference flow solver (FLUENT$^{\circledR}$). Numerical discretization schemes investigated include second order Central Differencing (CD), QUICK (Q), second order Upwind (2U), Bounded Central differencing (BCD) and first order upwind (1U). Turbulence closure models implemented include Smagorinsky

13

(SM), dynamic Smagorinsky (DSM) and Multiscale (MSM). Also implemented is the numerical LES technique Monotonically Integrated LES (MILES).

Results highlight the nonlinear interactions between different combinations of SGS closure models and discretization schemes. Further, results show that some combinations are more suitable than others. Favorable combinations identified as a result of the above were then tested for a high-Reynolds-number, momentum conserving, axisymmetric turbulent jet at Mach number 0.2. The results are compared in terms of mean velocity and turbulent shear stresses for different combinations. Also, comparisons are made in terms of the axial, radial and azimuthal components of turbulent (Reynolds) stress. Results indicate good agreement with the findings from the decaying turbulence simulations.

CHAPTER 3

PSEUDOSPECTRAL SIMULATION

3.1 Pseudospectral Simulations

3.1.1 Brief

In general, spectral methods can be classified as "interpolating" or "non-interpolating" types. Historically, the non-interpolating method was developed first. The difference between the two techniques lies in the method of evaluation of the coefficients of a given function. The interpolating method, i.e. Galerkin's method, is generally tedious to implement though results are of slightly higher fidelity. In using the non-interpolating type, the coefficients of a known function, *f(x)*, are multiplied by a given basis function and then numerically integrated.

Pseudospectral techniques are classified under the interpolating subgroup. Interpolating implies mathematically that a solver designed to perform a simulation of freely decaying turbulence on a domain Ω (consisting of a set of points) there is an association with a basis set. It follows that at each collocation (i.e. point) the differential equation is satisfied. By this, the coefficients of a known function *f(x)* are calculated by forcing the truncated series $f(x_i)$ to agree with *f(x)* at each point on Ω. Therefore as the number of points increases the truncated solution approaches the analytical solution [4].

Pseudospectral techniques are much simpler to implement and are also computation- ally more efficient than spectral (i.e. non-interpolating). For these reasons psedospectral methods have being adopted in this study. They are commonly used as a reliable alternative to performing higher fidelity non interpolating simulations of freely decaying turbulence. They are adopted here primarily because they enable isolation of SGS model error. That is, results from a pseudospectral simulation are in theory free of numerical error resulting from finite difference approximation of derivative.

3.1.2 Formulation

In this section the methodology is described for a simulation of decaying turbulence on a periodic box of size L and volume Ω. A three-dimensional infinite Fourier series representing pressure or velocity fluctuations can be written as:

$$f_i(\mathbf{x}) = \sum \hat{f}_i(\kappa) \exp\left[\imath\left(2\pi\kappa\mathbf{x}/L\right)\right] \tag{3.1}$$

where the summation is on wavevector $\kappa = \{k_1, k_2, k_3\}^T$ and $\imath = \sqrt{-1}$. For reasons such as memory limitations or cutoff wavenumber (k_c) requirements, the infinite Fourier series is truncated at the smallest scale of interest. For a homogeneous flow in three directions, defined on a domain Ω, the fluctuations must satisfy the incompressible equations:

$$\frac{\partial u_i}{\partial x_i} = 0, \tag{3.2}$$

$$\frac{\partial u_i}{\partial t} + \frac{\partial u_i u_j}{\partial x_j} = -\frac{\partial p}{\partial x_i} + \frac{\partial}{\partial x_j}\left(\nu\frac{\partial u_i}{\partial x_j}\right) \tag{3.3}$$

with periodic boundary conditions (BC) defined as:

$$u_i(\mathbf{x} + Le_i, t) = u_i(\mathbf{x}, t) \tag{3.4}$$

16

where e_i is the unit direction vector. Initial conditions (IC) are defined as as:

$$u_i(\mathbf{x}, t_0) = g_i(\mathbf{x}) \tag{3.5}$$

Substituting the truncated Fourier series into 3.3 gives the Fourier-Galerkin approximation to the NS equations:

$$\left(d/dt + \nu\kappa^2\right)\hat{u}_i(\kappa) = -\imath k_i \hat{p}(\kappa) - [\widehat{u_j u_{i,j}}](\kappa) \tag{3.6}$$

$$\imath\kappa_j \hat{u}_j(\kappa) = 0 \tag{3.7}$$

The term on the rightmost end of 3.6 can be represented as:

$$\hat{f}_i(\kappa) = -[\widehat{u_j u_{i,j}}](\kappa) \tag{3.8}$$

which is the Fourier series approximation of the convection term. Mathematically, 3.6 represents a convolution sum in Fourier space. It requires special treatment as discussed in a later section. By performing a contraction of 3.6, we can get a closed form solution to the Poisson equation for pressure in Fourier space:

$$\hat{p}(\kappa) = -\imath k_i \hat{f}_i / k^2 \tag{3.9}$$

Utilizing the continuity condition and substituting 3.9 into the momentum equation we have:

$$d\hat{u}_i(\kappa)/dt = -k_i k_j \hat{f}_j / k^2 - [\widehat{u_j u_{i,j}}](\kappa) + \nu\kappa^2 \hat{u}_i(\kappa) \tag{3.10}$$

Performing a large eddy simulation involves restricting 3.10 to account exclusively for large eddies. Mathematically this implies that a large eddy filter designed in a manner such as:

$$\bar{u}(\mathbf{x}) = \int_\Omega \bar{G}(\mathbf{x}, \acute{\mathbf{x}})u(\acute{\mathbf{x}})d\Omega \tag{3.11}$$

17

is applied to 3.10. $\bar{G}(\mathbf{x})$ is a filter typically specified as either Box, Gaussian or Sharp spectral. The modified equation, the filtered Navier Stokes equation including the subgrid stress (SGS) contribution to the flow field is:

$$d\hat{\bar{u}}_i(\kappa)/dt = -k_i k_j \hat{f}_i/k^2 - [\widehat{\bar{u}_i \bar{u}_{i,j}}](\kappa) + \nu\kappa^2 \hat{u}_i(\kappa) + \hat{\tau}_{ij,j} \qquad (3.12)$$

where the subgrid stress term:

$$\tau_{ij} = \bar{u}_i \bar{u}_j - \overline{u_i u_j} \qquad (3.13)$$

In practice, 3.12 is evolved in time on Ω using a suitable scheme. Here, 3.12 was evolved in time using the 2nd order Runge-Kutta scheme with a time step determined to be sufficiently small that time discretization errors were negligible. A number of researchers have proposed different methods for evaluating the SGS contribution to the large eddy flow field. In the pseudospectral simulation method the SGS term is evaluated in physical space, then Fast Fourier transformed to yield its spectral representation. The SGS models considered here are Smagorinsky (SM) [28], Dynamic Smagorinsky (DSM) [11], Multi-scale (MSM) [30] and the numerical LES method Monotonically Integrated LES (MILES) [10].

The least complex to formulate is the MILES model. In conventional SGS modeling, SGS models are formulated and explicitly incorporated into the Navier-Stokes equation for closure. Also, they serve as a route for which kinetic energy may be dissipated at high wavenumbers. Alternative to this is the MILES approach proposed by Fureby et al. [10], who argue that, conceptually, a model is accurate if it can properly route the kinetic energy out of the resolved eddies, preventing artificial energy pile up. In that case,

dissipation accounted for by the numerical flux formulation is sufficient. As implemented here, this implies that the eddy viscosity coefficient C_s is zero.

3.1.3 Error Analysis: On Numerical Error in Physical Space

As acknowledged by a number of researchers, the two major error sources present in performing LES of decaying turbulence using a finite volume solver are the SGS model and the discretization scheme. Discretization error can be subdivided into two categories, namely aliasing and numerical (i.e. truncation) error. The latter is a result of the order of accuracy of the discretization scheme. Kravchenko and Moin [16] assert that the principal source of numerical error in LES is error as a result of differentiation of the nonlinear (convective) term. Based on this, numerical error representation in physical space using the convective form of the nonlinear term, 2.7, can be formulated as follows. Given 2.7, first specify an operator defined as:

$$\frac{\delta}{\delta x_j} = \left(\frac{\partial}{\partial x_j}\right)_{EXACT} - \left(\frac{\partial}{\partial x_j}\right)_{DISCRETIZED} \qquad (3.14)$$

The numerical error in physical space is then simply expressed as:

$$e_i = \bar{u}_j \frac{\delta \bar{u}_i}{\delta x_j} \qquad (3.15)$$

For a structured mesh we define a one dimensional (1D) control volume as shown in Figure 3.1. Let ϕ_e and ϕ_w represent a convected variable on the east and west face
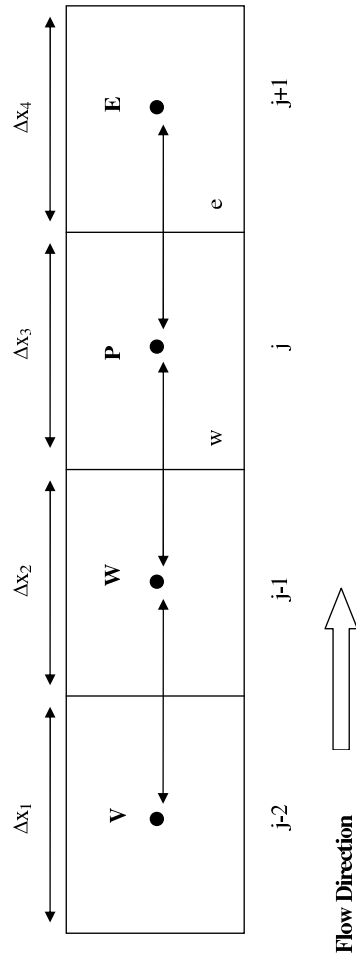
Figure 3.1

See appendix for details

surrounding point P, respectively. For a flow moving from west to east, the convected variable on the east and west faces can be represented by a general formulation:

$$\phi_e = \theta \left[\frac{\Delta x_4}{\Delta x_3 + \Delta x_4} \phi_P + \frac{\Delta x_3}{\Delta x_3 + \Delta x_4} \phi_E \right] + (1-\theta) \left[\frac{\Delta x_2 + 2\Delta x_3}{\Delta x_2 + \Delta x_3} \phi_P - \frac{\Delta x_3}{\Delta x_2 + \Delta x_3} \phi_W \right]$$

(3.16)

$$\phi_w = \theta \left[\frac{\Delta x_3}{\Delta x_2 + \Delta x_3} \phi_W + \frac{\Delta x_2}{\Delta x_2 + \Delta x_3} \phi_P \right] + (1-\theta) \left[\frac{\Delta x_1 + 2\Delta x_2}{\Delta x_1 + \Delta x_2} \phi_W - \frac{\Delta x_2}{\Delta x_1 + \Delta x_2} \phi_V \right]$$

(3.17)

where ϕ_V, ϕ_W, ϕ_P and ϕ_E are known values of the function at their respective nodal points. This formulation describes a family of 2nd order discretization schemes, each specified by a particular value of θ, which determines the degree of upwinding. For example, a value of $\theta = 1$ yields the central difference scheme, and a value of $\theta = 0$ yields the second-order upwind scheme [1]. If a uniform grid spacing is assumed then $\Delta x_1 = \Delta x_2 = \Delta x_3 = \Delta x_4 = \Delta x_i$. Considering the central difference scheme as an example, then $\theta = 1$ and for any value of Δx_i, the derivative at point P is approximated as:

$$\frac{d\phi}{dx} = \frac{\phi_e - \phi_w}{\Delta x_i}$$

(3.18)

where the convected variable on the faces are:

$$\phi_e = \frac{1}{2}\phi_P + \frac{1}{2}\phi_E$$

(3.19)

and:

$$\phi_w = \frac{1}{2}\phi_W + \frac{1}{2}\phi_P$$

(3.20)

21

Deriving a Taylor series expansion for function values ϕ_P ϕ_E and ϕ_W noting that ϕ_W, ϕ_P, ϕ_E are at the j-1, j, and j+1 positions, respectively, as depicted on Figure 3.1, yield the following:

$$\phi_W = u_j + u_x \Delta x + u_{xx} \frac{\Delta x^2}{2} + u_{xxx} \frac{\Delta x^3}{6} + u_{xxxx} \frac{\Delta x^4}{24} +$$
$$u_{xxxxx} \frac{\Delta x^5}{120} + u_{xxxxxx} \frac{\Delta x^6}{720} + u_{xxxxxxx} \frac{\Delta x^7}{5040} + \ldots + \tag{3.21}$$

$$\phi_P = u_j \tag{3.22}$$

$$\phi_E = u_j - u_x \Delta x + u_{xx} \frac{\Delta x^2}{2} - u_{xxx} \frac{\Delta x^3}{6} + u_{xxxx} \frac{\Delta x^4}{24} -$$
$$u_{xxxxx} \frac{\Delta x^5}{120} + u_{xxxxxx} \frac{\Delta x^6}{720} - u_{xxxxxxx} \frac{\Delta x^7}{5040} + \ldots + \tag{3.23}$$

Substituting 3.21-3.23 into 3.19 and 3.20:

$$\phi_w = u_j + u_x \frac{\Delta x}{2} + u_{xx} \frac{\Delta x^2}{4} + u_{xxx} \frac{\Delta x^3}{12} + u_{xxxx} \frac{\Delta x^4}{48} +$$
$$u_{xxxxx} \frac{\Delta x^5}{240} + u_{xxxxxx} \frac{\Delta x^6}{1440} + u_{xxxxxxx} \frac{\Delta x^7}{10080} + \ldots + \tag{3.24}$$

and:

$$\phi_e = u_j - u_x \frac{\Delta x}{2} + u_{xx} \frac{\Delta x^2}{4} - u_{xxx} \frac{\Delta x^3}{12} + u_{xxxx} \frac{\Delta x^4}{48} -$$
$$u_{xxxxx} \frac{\Delta x^5}{240} + u_{xxxxxx} \frac{\Delta x^6}{1440} - u_{xxxxxxx} \frac{\Delta x^7}{10080} + \ldots + \tag{3.25}$$

respectively . To develop an expression for the numerical error as a result of implementing the central differencing scheme, it follows from substitution of 3.24 and 3.25 into 3.18 that:

$$\frac{d\phi}{dx} = u_x + u_{xxx} \frac{\Delta x^2}{6} + u_{xxxxx} \frac{\Delta x^4}{120} + u_{xxxxxxx} \frac{\Delta x^6}{5040} + \ldots + \tag{3.26}$$

Rewriting 3.26 we have:

$$\frac{d\phi}{dx} - u_x = u_{xxx}\frac{\Delta x^2}{6} + u_{xxxxx}\frac{\Delta x^4}{120} + u_{xxxxxxx}\frac{\Delta x^6}{5040} + \ldots + \tag{3.27}$$

The truncation error is defined in terms of the difference between the continuous derivative and the discrete (numerical) approximation of the derivative $\frac{d\phi}{dx}$. Employing the operator defined in 3.14, the following result is obtained:

$$\frac{\delta^{CD}}{\delta x} = u_{xxx}\frac{\Delta x^2}{6} + u_{xxxxx}\frac{\Delta x^4}{120} + u_{xxxxxxx}\frac{\Delta x^6}{5040} + \ldots + \tag{3.28}$$

The error operator associated with the resolved (filtered) velocity field is expressed as:

$$\frac{\delta^{CD}}{\delta x} = \bar{u}_{xxx}\frac{\Delta x^2}{6} + \bar{u}_{xxxxx}\frac{\Delta x^4}{120} + \bar{u}_{xxxxxxx}\frac{\Delta x^6}{5040} + \ldots + \tag{3.29}$$

Similarly, for $\theta = 0, 1/8$ corresponding to the second order Upwind (2U) [2, 32] and QUICK (Q) [17] schemes, the numerical error operator is equal to:

$$\frac{\delta^{2U}}{\delta x} = \bar{u}_{xxx}\frac{\Delta x^2}{3} + \bar{u}_{xxxx}\frac{\Delta x^3}{4} + \bar{u}_{xxxxx}\frac{7\Delta x^4}{60} + \ldots + \tag{3.30}$$

$$\frac{\delta^{Q}}{\delta x} = \bar{u}_{xxx}\frac{13\Delta x^2}{48} + \bar{u}_{xxxx}\frac{7\Delta x^4}{32} + \bar{u}_{xxxxx}\frac{97\Delta x^4}{760} + \ldots + \tag{3.31}$$

The Fourier-Galerkin approximation to the NS equations is modified to include the effects of finite-difference error by adding the error term defined by 3.15:

$$d\hat{\bar{u}}_i(\kappa)/dt = -k_i k_j \hat{f}_i/k^2 - [\widehat{\bar{u}_i \bar{u}_{i,j}}](\kappa) + \nu\kappa^2 \hat{u}_i(\kappa) + \hat{\tau}_{ij,j} + \hat{e}_i(\kappa) \tag{3.32}$$

The operator $\frac{\delta}{\delta x_j}$ for any particular scheme is obtained using expressions of the form 3.29-3.31. The derivatives appearing in these terms are computed directly from the Fourier representation of the velocity field at each time step. For the pseudospectral approach adopted

23

here, the error terms are evaluated similar to the SGS modeling terms. The velocity field is first transformed to physical space using the Inverse Fourier Fast Transform. The error terms $\hat{e}_i$ are then evaluated at each grid point in physical space, and transformed back to wavenumber space using the Fast Fourier Transform. It should also be noted that for the case of second order upwind and QUICK shemes, their upwinding nature was preserved in the simulations by multiplying the even components of 3.30 and 3.31 by the absolute value of the filtered velocities, when computing the error term $\hat{e}_i$. In practice, the infinite Fourier series representation of the numerical error is truncated to a finite number of terms. Numerical experiments were performed to determine the appropriate number of terms for accurate representation of the numerical error, and are discussed further in chapter V.

3.2   Considerations

3.2.1   Initial and Boundary Conditions

Constructing initial conditions for simulating freely decaying isotropic turbulence requires that on the given domain Ω the velocity field satisfy these basic criteria:

1. The velocity field must satisfy conservation of mass
2. The velocity field must be physically meaningful
3. The energy spectrum of the velocity field must be realistic

To address these three criteria, we first define three random phase angles, (e.g. with the rand() function on a Fortran platform) $\theta_1(\kappa), \theta_2(\kappa)$ and $\phi(\kappa)$ for $\kappa = \sqrt{k_i k_i}$, specifying $\kappa_{12} = \sqrt{k_1^2 + k_2^2}$. Using the representative energy spectrum:

$$E(\kappa) = C_k \epsilon^{2/3} k^{-5/3} (k\ell (k\ell^{\alpha_2} + \alpha_1)^{1/\alpha_2})^{5/3+\alpha_3} \exp(-\alpha_4 k\eta)$$

$$(1 + \alpha_5(1/\pi \arctan(\alpha_6 log(k\eta) + \alpha_7) + 0.5)) \tag{3.33}$$

prescribed by Kang et al. [15], we define a piecewise continuous three dimensional velocity field in Fourier space following the suggestions of Rogallo [26]:

$$\hat{u}_1(\kappa) = \begin{cases} \alpha(\kappa) & if\ k_{12} = 0 \\ (\alpha(\kappa)kk_2 + \beta(\kappa)k_1k_3)/(kk_{12}) & otherwise \end{cases} \tag{3.34}$$

$$\hat{u}_2(\kappa) = \begin{cases} \beta(\kappa) & if\ k_{12} = 0 \\ (\beta(\kappa)k_2k_3 - \alpha(\kappa)kk_1)/(kk_{12}) & otherwise \end{cases} \tag{3.35}$$

$$\hat{u}_3(\kappa) = \begin{cases} 0 & if\ k_{12} = 0\ and\ k_3 = 0 \\ \beta(\kappa)k_{12}/k & if\ k_{12} \neq 0\ and\ k_3 = 0 \\ -(k_1\hat{u}_1 + k_2\hat{u}_2)/k_3 & otherwise \end{cases} \tag{3.36}$$

using the quantities:

$$\alpha(\kappa) = \sqrt{E(k)/2\pi k^2} \exp(\imath 2\pi\theta_1(\kappa)) \cos(2\pi\phi(\kappa)) \tag{3.37}$$

$$\beta(\kappa) = \sqrt{E(k)/2\pi k^2} \exp(\imath 2\pi\theta_2(\kappa)) \sin(2\pi\phi(\kappa)) \tag{3.38}$$

The following symmetry condition was utilized so that the simulation required computation of only fifty percent of the entire velocity field.

$$\hat{u}_i(\kappa) = \hat{u}_i^*(-\kappa) \tag{3.39}$$

The above described initial velocity field is an approximation of a turbulent flow but with random phases for each wavenumber mode. In practice, this leads to an initial transient behavior during which the phases adjust and the velocity field becomes representative of a turbulent flowfield.

25

3.2.2 Aliasing Error

Issues regarding aliasing account for most of the computational difficulties encountered in evolving the filtered Navier Stokes equations in spectral space. Aliasing error in spectral space arises as a result of the nonlinear term representing a convolution sum for a quadratic non-linearity. The nonlinear term is expressed as:

$$\hat{f}_i(\kappa) = \sum_{\kappa=\kappa'+\kappa''} -\imath k_j'' \hat{u}_i(\kappa') \hat{u}_i(\kappa'') \tag{3.40}$$

Consider a quadratic non-linearity defined on a discretized domain $x_j \in [0, 2\pi)$. The discrete transforms:

$$U_j = \sum_{k=N/2}^{N/2-1} \hat{u}_k e^{\imath k x_j} \tag{3.41}$$

$$V_j = \sum_{k=N/2}^{N/2-1} \hat{v}_k e^{\imath k x_j} \tag{3.42}$$

where the product gives:

$$W_j = U_j V_j \tag{3.43}$$

for index j defined on $[0, 1, \ldots, N-1]$ where $x_j = 2\pi j/N$. The Fourier transform of product 3.43 is:

$$\hat{W}_k = \frac{1}{N} \sum_{j=0}^{N-1} W_j e^{\imath k x_j} \tag{3.44}$$

Using the orthogonality relation:

$$\frac{1}{N} \sum_{j=0}^{N-1} e^{\imath k x_j} = \begin{cases} 1 & if \ p = Nm \ for \ m = \pm1, \pm2, \ldots \\ \\ 0 & otherwise \end{cases} \tag{3.45}$$

We can rewrite 3.44 as:

$$\hat{W}_k = \sum_{m+n=k} \hat{u}_m \hat{v}_n + \sum_{m+n=k\pm N} \hat{u}_m \hat{v}_n = \hat{w}_k + \sum_{m+n=k\pm N} \hat{u}_m \hat{v}_n \tag{3.46}$$

The first term of 3.46 is simply the term that results from truncating the infinite Fourier series of the convolution sum. The second term is responsible for aliasing coefficients of wavenumber modes outside of the truncated range $|k| \leq \frac{N}{2}$, leading to aliasing error. Since aliasing error can quickly contaminate a solution several techniques have being developed to address aliased modes [5]. A common technique, as that implemented here, is the $\frac{3}{2} - Rule$. It requires 150 percent more grid points in each coordinate direction. It involves extending the domain from N to $M = \frac{3}{2}N$, implying that $\frac{-M}{2} \leq k \leq \frac{M}{2} - 1$. It follows that the new discrete transforms defined by:

$$U_j = \sum_{k=M/2}^{M/2-1} \tilde{u}_k e^{\imath k x_j} \begin{cases} \tilde{u}_k = \hat{u}_k & if \, |k| \leq \frac{N}{2} \\ \\ 0 & otherwise \end{cases} \tag{3.47}$$

$$V_j = \sum_{k=M/2}^{M/2-1} \tilde{v}_k e^{\imath k x_j} \begin{cases} \tilde{v}_k = \hat{v}_k & if \, |k| \leq \frac{N}{2} \\ \\ 0 & otherwise \end{cases} \tag{3.48}$$

will completely addresses aliasing error as a result the convolution sum of the quadratic nonlinearity. Zero padding modes outside the subrange ensures an aliased-free solution.

3.3 Test Case

3.3.1 Experimental Parameters

LES of freely decaying isotropic turbulence owes its principal point of reference to the classical experimental data of Comte-Bellot and Corrsin [7] (CBC). However, as highlighted by several experimentalists in the area of decaying turbulence, the limitations of the investigations of CBC include a low-Reynolds-number, $(Re_\lambda \approx 150)$ and a lack of higher order statistics. These limitations have inspired subsequent investigation and sev-

27

eral have been pursued. The experimental data set considered here is the investigation of Kang et al. [15] which serves as an update of the CBC investigations.

Kang et al. [15] document an experimental study of high-Reynolds number, $630 \leq Re_\lambda \leq 720$, isotropic turbulence. They were able to circumvent the Reynolds number limitations by incorporating active grid systems following "in-plane orientation" of Makita [18], and Mydlarski and Warhaft [20, 21]. Though not of interest in the current study, higher-order statistics were obtained following the implementation of Cerutti et al. [6] using an array of X-wire probes.

Measurements were taken at four downstream locations in the wind tunnel. Far behind the active grid, they measured a streamwise to transverse velocity ratio of approximately 1.15. Indicating that the turbulence was nearly isotropic. Dissipation rate, ϵ, at successive positions was measured from the decay rate of kinetic energy. Following the suggestion of Pope [24], since the three-dimensional and longitudinal spectra are related by:

$$E_{11}(\kappa_1) = \int_1^\infty \frac{x^2 - 1}{x^3} E(\kappa x) dx \tag{3.49}$$

$$E_{22}(\kappa_1) = 0.5 \int_1^\infty \frac{x^2 + 1}{x^3} E(\kappa x) dx \tag{3.50}$$

where $x = \frac{\kappa}{\kappa_1}$, the three-dimensional spectra was found by a trial and error method, accounting for limiting conditions and bypassing differentiation. It was found to agree with a fitting function of the form:

$$E(\kappa) = C_k \epsilon^{2/3} k^{-5/3} \left[\frac{k\ell}{(k\ell)^{\alpha_2} + \alpha_1)^{1/\alpha_2}} \right]^{5/3+\alpha_3} \exp(-\alpha_4 k\eta)$$
$$\left[1 + \alpha_5 (\frac{1}{\pi} \arctan(\alpha_6 log(k\eta) + \alpha_7) + \frac{1}{2}) \right] \tag{3.51}$$

where the integral and Kolmogrov length scale are denoted as ℓ and η. For $i = 1, ..., 7$, $\alpha_i = 0.39, 1.2, 4.0, 2.1, 0.522, 10.0, 12.58$, respectively, and $C_k = 1.613$. $Table$ 3.1 shows measured flow properties, at successive measurement locations, used for developing the numerical parameters for the simulations corresponding to this test case.

Table 3.1

Experimental Parameters from Kang et al. [15]

$\frac{x_1}{M}$	20	30	40	48
$\langle u_1 \rangle \, (ms^{-1})$	12.0	11.2	11.0	10.8
$u_{1r.m.s}(ms^{-1})$	1.85	1.43	1.19	1.08
$u_{2r.m.s}(ms^{-1})$	1.64	1.25	1.04	0.932
$I = u_{1r.m.s}/u_{2r.m.s}$	1.13	1.14	1.14	1.16
$\epsilon(m^2 s^{-3})$	22.8	9.13	4.72	3.14
$\ell(m)$	0.250	0.288	0.321	0.322
$\eta(mm)$	0.11	0.14	0.16	0.18
$R_{eM} = \langle u_1 \rangle M/\nu$	1.21E5	1.13E5	1.11E5	1.09E5
$R_{e\lambda} = u_{1r.m.s}\lambda/\nu$	716	676	650	626
$R_{e\ell} = u_{1r.m.s}\ell/\nu$	30,600	27300	25300	23700

3.3.2 Numerical Parameters

LES of isotropic turbulence was performed following the experiments of Kang et al. [15]. Numerical simulation parameters were developed from the experimental data collected at four downstream positions; $\frac{x}{M} = 20, 30, 40, 48$. Taylor's hypothesis:

$$t = \int_0^x \frac{dx}{\langle u_1 \rangle (x)} \tag{3.52}$$

3.52, was invoked to convert spatial decay in the experimental wind tunnel to temporal decay in the computational domain Ω. Numerical simulations were initialized using the

29

energy spectrum fitting function corresponding to data collected at non-dimensional distance $\frac{x_1}{M} = 20$ where $M = 0.152$. The the non-dimensional quantities used were scaled according to the numerical simulation parameters implemented by Kang et al. [15] in comparison with their experimental data. The non-dimensional length was:

$$l^* = \frac{L_{EXP}}{S_\Omega} = 0.8148733 \tag{3.53}$$

where the numerical periodic box used is of size $S_\Omega = 2\pi(m)$ and $L_{EXP} = 5.12(m)$. The velocity scale chosen for non-dimentionalization is $\langle u_{ref} \rangle_{r.m.s} = 2(m/s)$. By inspection of $Table$ 3.1 it is apparent that the choice of $\langle u_{ref} \rangle_{r.m.s}$ is appropriate for an upper bound of longitudinal velocity. It follows that:

$$u^* = \frac{max \, \langle u_1 \rangle_{r.m.s}}{\langle u_{ref} \rangle_{r.m.s}} = 0.925 \tag{3.54}$$

From this, the computational Reynolds number is found to be:

$$Re_{CMP} = \frac{Re_{EXP}}{u^* l^*} = \frac{u_{1r.m.s} M}{\nu u^* l^*} = 2.47E4 \tag{3.55}$$

where $M = 0.152$ is the grid size of the experimental mesh rods. Non-dimensional time scale is found to be:

$$t^* = \frac{l^*}{u^*} = 0.881 \tag{3.56}$$

from which a turbulent time scale can be calculated also using $Table$ 3.1. This is:

$$\tau_{turb,EXP} = \frac{u_{1r.m.s}^2}{\epsilon} = 0.15011 \tag{3.57}$$

From there, the corresponding numerical turbulent time scale can be computed which is:

$$\tau_{turb,NUM} = \frac{\tau_{turb,EXP}}{t^*} = 0.17026 \tag{3.58}$$

30

From Kang et al. [15], the experimental timestep size is $\Delta t_{EXP} = .000163(s)$. Since the

computational domain evolved in time is of sizes 32^3 and 64^3, we have a numerical time

step size of:

$$\Delta t_{NUM,32^3} = \frac{\Delta t_{EXP} * \tau_{turb,EXP}}{\tau_{turb,NUM}} = .00074 \qquad (3.59)$$

and:

$$\Delta t_{NUM,64^3} = \frac{\Delta t_{EXP} * \tau_{turb,EXP}}{\tau_{turb,NUM}} = 0.00037 \qquad (3.60)$$

respectively. $Table$ 3.2 shows other numerical parameters obtained for the pseudospectral

LES of isotropic decaying turbulence.

Table 3.2

Simulation Parameters for LES of Isotropic Decaying Turbulence

$\frac{x_1}{M}$	20	30	40	48
$\langle u_1 \rangle \, (ms^{-1})$	12.0	11.6	11.1	10.9
$Run\ Time\ T = \Delta x_1 / \langle u_1 \rangle \, \tau_{turb,EXP}$	0	0.1491	0.3049	.4318
$Number\ of\ iteration,\ N = T/\Delta t$	Start	403	824	1167
$Integral\ scale,\ \ell = \ell_{EXP}/\ell^*$	0.3068	0.3534	0.39393	0.4074
$\eta = \eta_{EXP}/\ell^*$	1.35E-4	1.72E-4	1.9635E-4	2.209E-4
ϵ	23.4747	9.40017	4.8597	3.511

CHAPTER 4

FINITE VOLUME SIMULATIONS

4.1 Methodology

The purpose of the finite volume simulations is to verify that the observations made using the modified psuedospectral code as a tool for determining favorable combinations of closure models with numerical schemes hold for simulations in physical space. Therefore, the finite volume simulations were performed with equivalent specification as those of the pseudospectral simulations. Details are discussed in the following sections. Simulations were conducted using a commercially available finite volume solver, FLUENT$^{\textregistered}$ (Fluent, Inc., Lebanon, NH).

4.2 Simulation Details

A cube size of 2.56m discretized into 64^3 uniform finite volumes was used for the computational domain. A fully implicit solution algorithm was implemented with time advancement achieved using a 2nd order backward differencing approximation. Non-dimensional time stepsize (equation 3.60) used is that determined following Kang et al. [15], and is identical to that applied in the pseudospectral simulations. Simulations were also performed using a smaller (by one half) step size to confirm that the chosen time step was sufficiently small that it had negligible effects on the results. The governing equations

for finite-volume LES were solved using a segregated solver: continuity and momentum were solved in a decoupled manner during each outer iteration. Because of its computational efficiency, the non-iterative time advancement (NITA) technique was used instead of an iterative method. The fractional step method was used for pressure-velocity coupling. Figure 4.1 is a plot of the evolution of turbulent kinetic energy versus time, comparing the iterative and non-iterative methods. It demonstrates that the non iterative technique gives comparable results to that of an iterative method using the SIMPLE scheme for pressure-velocity coupling. The NITA technique was found to require approximately one order of magnitude less computational time than the SIMPLE scheme.

Pressure at the control volume faces was computed using a second order extrapolation method. The convective fluxes were evaluated using second order spatial discretization schemes. Discretization schemes used include the 2nd order upwind (2U), central differencing (CD) and QUICK (Q) schemes. In addition, the second order bounded central differencing (BCD), available exclusively in FLUENT$^{\textcircled{R}}$, as well as the 1st order upwind (1U) schemes were investigated. The BCD scheme is a piecewise adaptive scheme which is 1U in regions where the convective boundedness criteria is violated and combined CD and 2U otherwise. It has been proposed that the BCD scheme offers satisfactory results at high wavenumber regions, unlike the unbounded non physical energy concentration in simulations implemented using CD scheme [23].

Subgrid stress modeling was achieved using the Smagorinsky (SM) [28], dynamic Smagorinsky (DSM) [11], Monotonically Integrated LES (MILES) [10] and the Multi-scale (MSM) [30] techniques. In FLUENT$^{\textcircled{R}}$, the MILES technique was implemented

simply by specifying a zero eddy viscosity coefficient, $C_s = 0$. The initial velocity field

was generated using techniques described by [31] with the energy spectrum specified by

equation 3.51, using 30 discrete wavenumbers ranging from the Kolmogrov scale, η, to 10

times the integral scale, ℓ, logarithmically equispaced with a ratio of 1.122. Also, since

volume averaging corresponds to convolution of the velocity field with a box filter, the box

filtering was accounted for by prescribing an energy spectrum corresponding to:

$$E_{filt}(\kappa) = G^2(\kappa)E(\kappa) = \left[\frac{sin(\kappa\Delta)}{\kappa\Delta}\right]^2 E(\kappa) \tag{4.1}$$
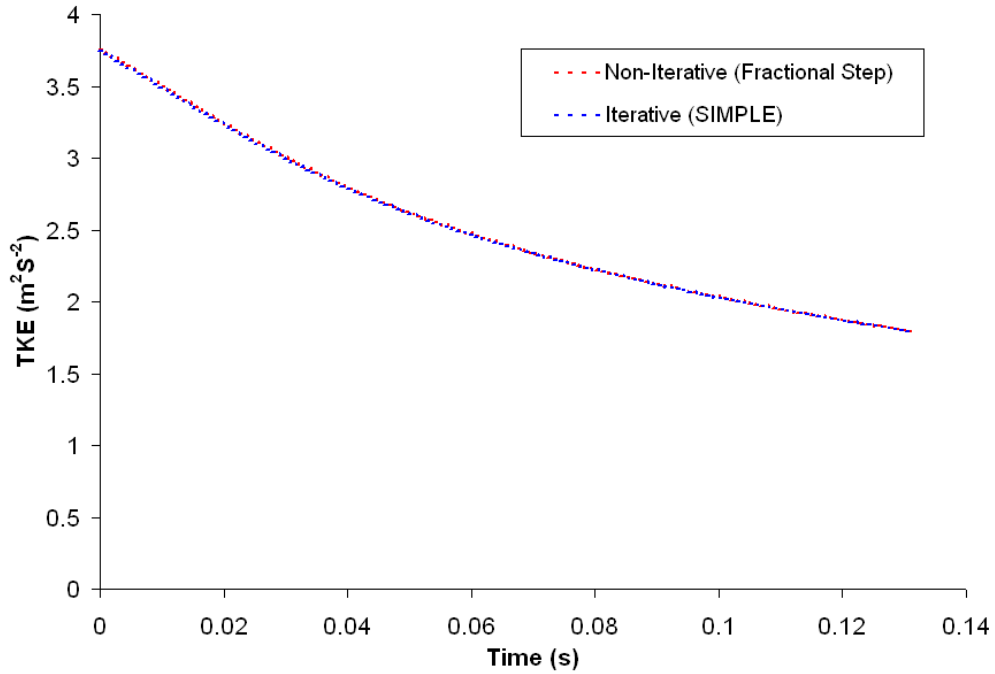
Figure 4.1

See appendix for details

where $E(\kappa)$ is the energy spectrum defined by 3.51 and $G(\kappa)$ is the box filter kernel.

34

CHAPTER 5

RESULTS

5.1 Results

5.1.1 Brief

The goal of this research effort is to determine best practice guidelines for performing finite-volume LES of flows in configurations of engineering interest. The approach taken to achieve this research goal is as follows. The two sources of error present in performing finite-volume large eddy simulation (FV-LES) are SGS modeling and numerical error. SGS modeling error can be isolated by performing LES using pseudospectral techniques. As established by Kravchenko and Moin [16], the bulk of numerical error present in performing FV-LES is due to numerical differentiation of the non-linear term. It should be noted that, for reasons such as implementation difficulties in complex geometries etc, pseudospectal techniques are not commonly tailored into general-purpose or commercial CFD solvers. This study proceeds by deriving a Taylor series expansion of numerical error present in FV-LES codes for CD, 2U and Q schemes. Following this, the spectral representation of numerical error in physical space is explicitly incorporated into a previously validated dialiased pseudospectral code [3]. Using the modified pseudospectral code, LES of isotropic turbulence is carried out on domain sizes 32^3 and 64^3. For verification, finite

volume simulations are also carried out with similar specifications as those of the pseudospectral simulations.

5.2   Pseudospectral Simulation Results

For the pseudospectral simulations, it was first necessary to determine the appropriate number of terms needed to be retained in the Taylor series expansion of the numerical error term (Equations 3.29-3.31). To do this, simulations were conducted using a successively larger number of terms to represent the numerical differentiation error. Figures 5.1 and 5.2 show that after the third truncation error term there is no significant change in the computed energy density spectrum using the 2U and CD schemes. Although not shown, similar results were obtained for the QUICK scheme. As a result of these findings, equation 3.29 was truncated after the seventh derivative term and further denoted as SM-CD.

A similar approach was taken for equations 3.30 and 3.31, i.e. they were truncated after the fifth derivative term, which is the third non-zero term in the series. The naming convection used in the remainder of this section is as follows. A label such as DSM implies pure pseudospectral LES with dynamic Smagorinsky SGS model. DSM-CD implies LES pseudospectral simulation of dynamic Smagorinsky SGS model with (truncated) error contribution from the CD numerical flux formulation.

Figure 5.3 shows results from LES on the 32^3 grid using the Smagorinsky SGS model in conjunction with numerical error from three numerical flux formulations. The results highlight the dissipative nature of the upwind biased schemes.This effect is most apparent at higher wavenumbers where the result clearly indicate that there is an excessive removal

36
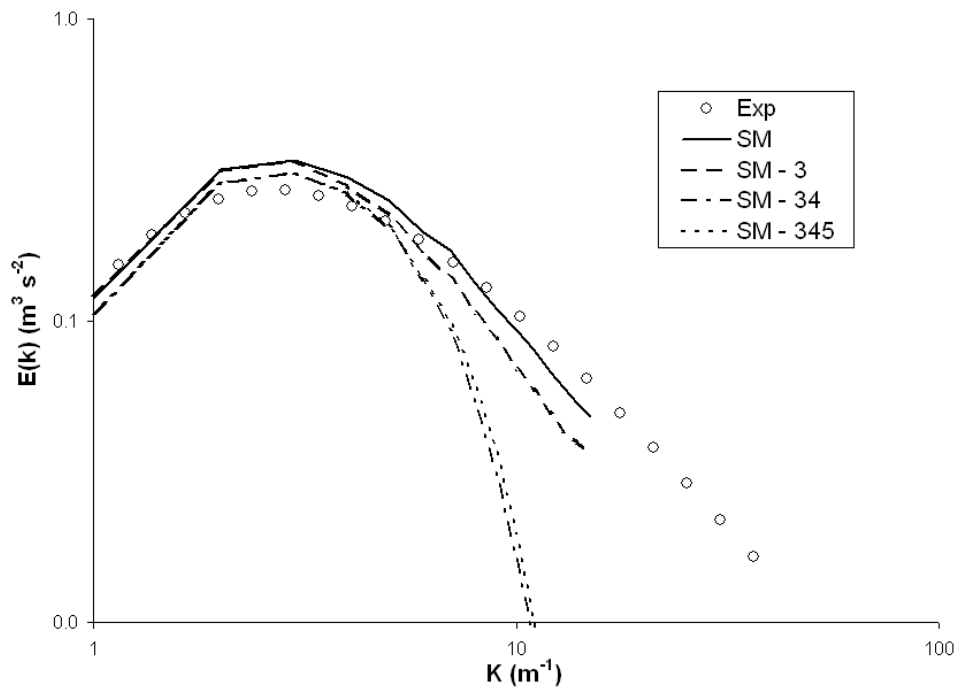
Figure 5.1

See appendix for details
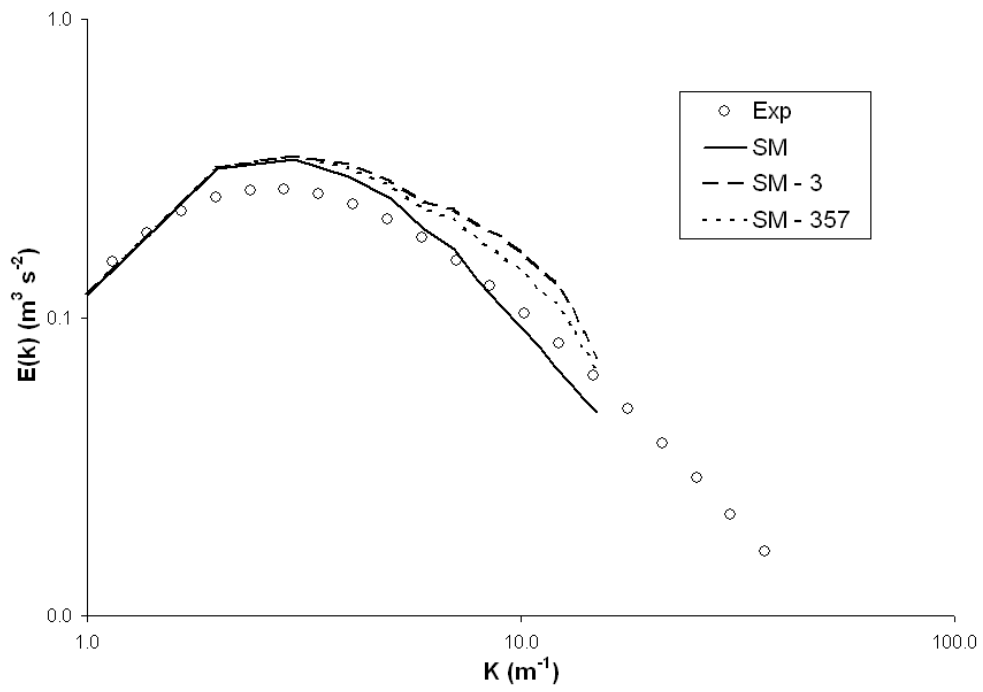
Figure 5.2

See appendix for details

of energy indicated by the underprediction of the experimental data. The SM-CD gives

results contrary to this. It shows an eccessive pile up of energy at high wavenumbers. A

similar phenomenon occurs on a much refined grid, Figure 5.4. For this case, the disper-

sion effect of the central difference scheme clearly dominates the dissipation influence of

the SGS model, leading to significant overprediction of energy at high wavenumbers.
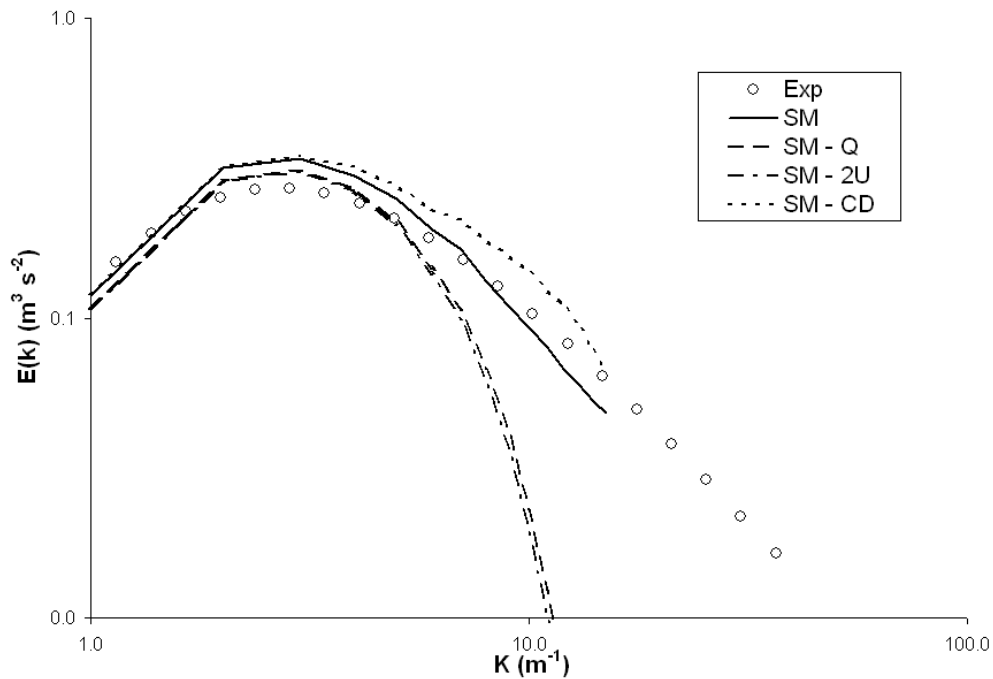
Figure 5.3

See appendix for details

The dynamic Smagorinsky SGS model in conjunction with numerical error from the

upwind biased schemes, Figures 5.5 and 5.6, likewise shows a similar trend to the results

obtained using the Smagorisky model, Figures 5.3 and 5.4. It is important to note that
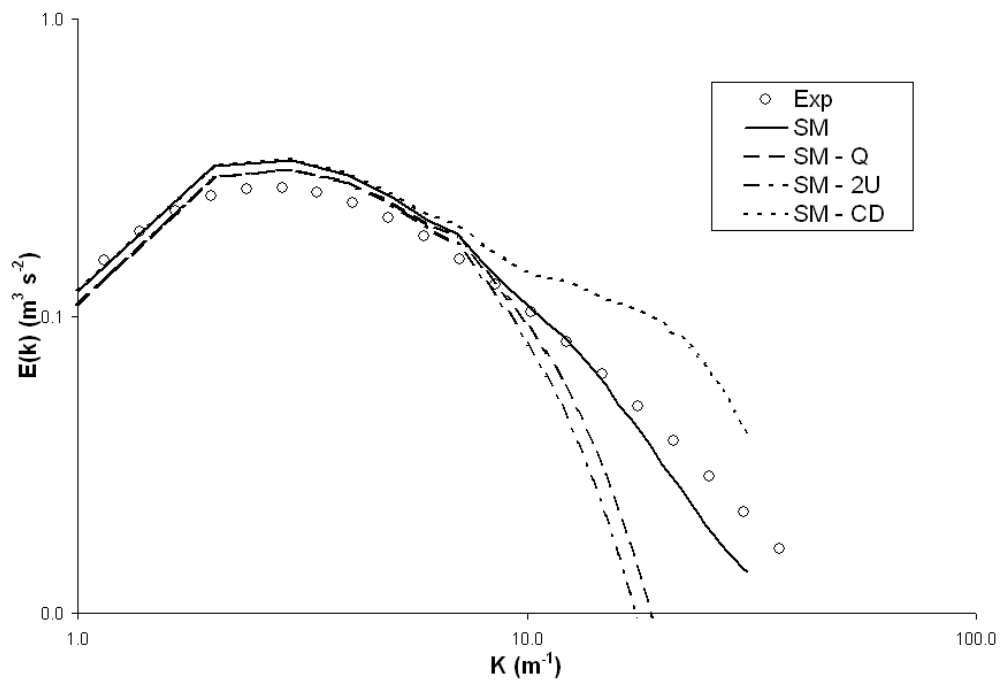
Figure 5.4

See appendix for details

the solution diverged for the combination of dynamic Smagorinsky SGS model with central differencing, DSM-CD. This can be attributed to excess dispersion and non-physical energy at high wavenumbers from the numerical scheme. This occurrence clearly demonstrates the nonlinear interaction between SGS models and numerical flux formulations. The eddy viscosity coefficient in the dynamic model is dependent on the resolved strain-rate rather than on a fixed coefficient as in the case of the Smagorinsky model and the dissipative influence of this model is not sufficient to stabilize the dispersive effect of the CD scheme.
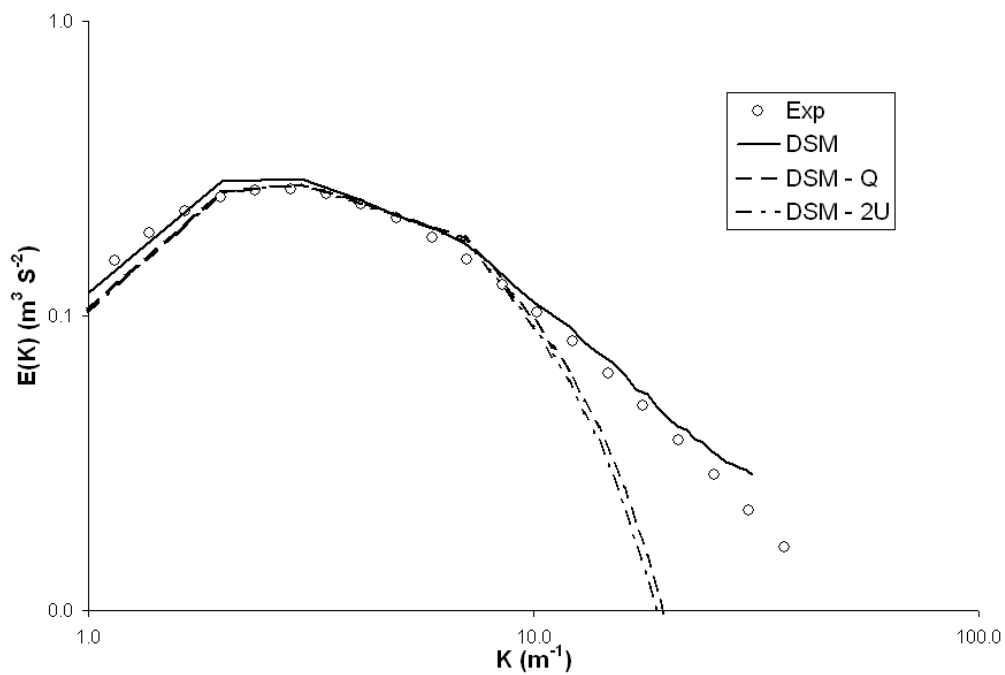
Figure 5.5

See appendix for details
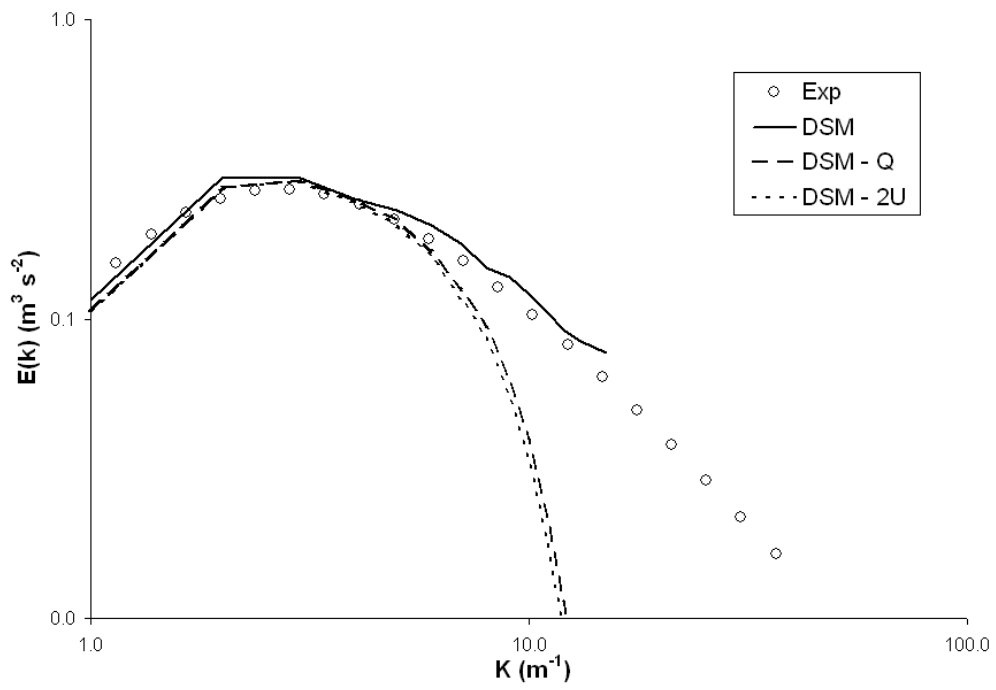
Figure 5.6

See appendix for details

The multiscale model, Figure 5.7, in combination with the three flux formulations also shows similar trends as the dynamic Smagorisky and Smagorinsky cases. As shown in Figure 5.8, the multiscale model results are almost identical to the Smagorinsky model results. This is expected since the MSM model was calibrated to give similar results as the SM model for decaying isotropic turbulence [30].
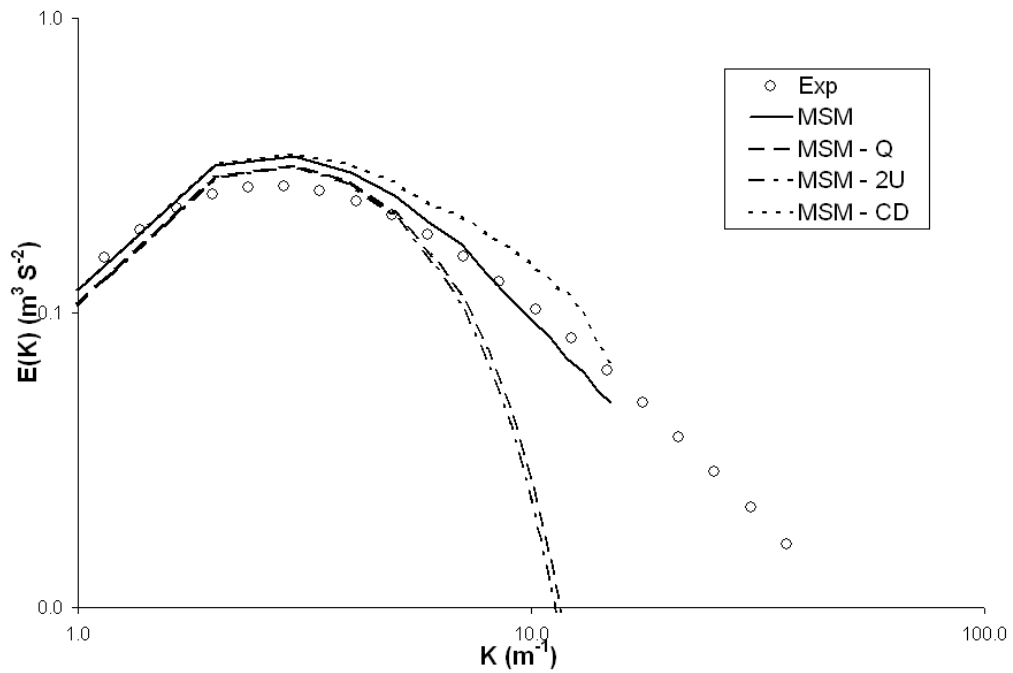
Figure 5.7

See appendix for details

The MILES approach in conjunction with numerical error from the upwind biased schemes, Figure 5.9, likewise shows a similar trend to the results obtained using the Smagorisky model. Similar to the dynamic Smagorisky cases, Figures 5.5 and 5.6, the so-
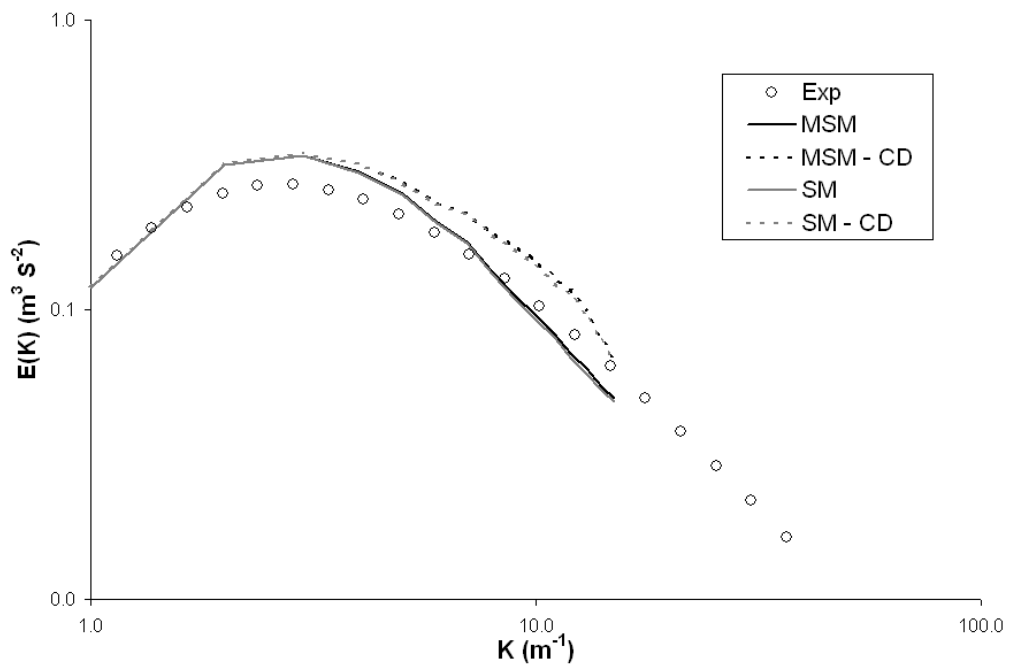
Figure 5.8

See appendix for details

lution diverged for the combination of MILES technique with central differencing, MILES-CD. This can also be attributed to excess dispersion and non-physical energy at high wavenumbers from the numerical scheme. This reinforces the nonlinear interaction between SGS models and numerical flux formulations. The eddy viscosity coefficient for the MILES approach is set to zero. This approach is not sufficient to stabilize the dispersive effect of the CD scheme since it has a zero dissipative influence.
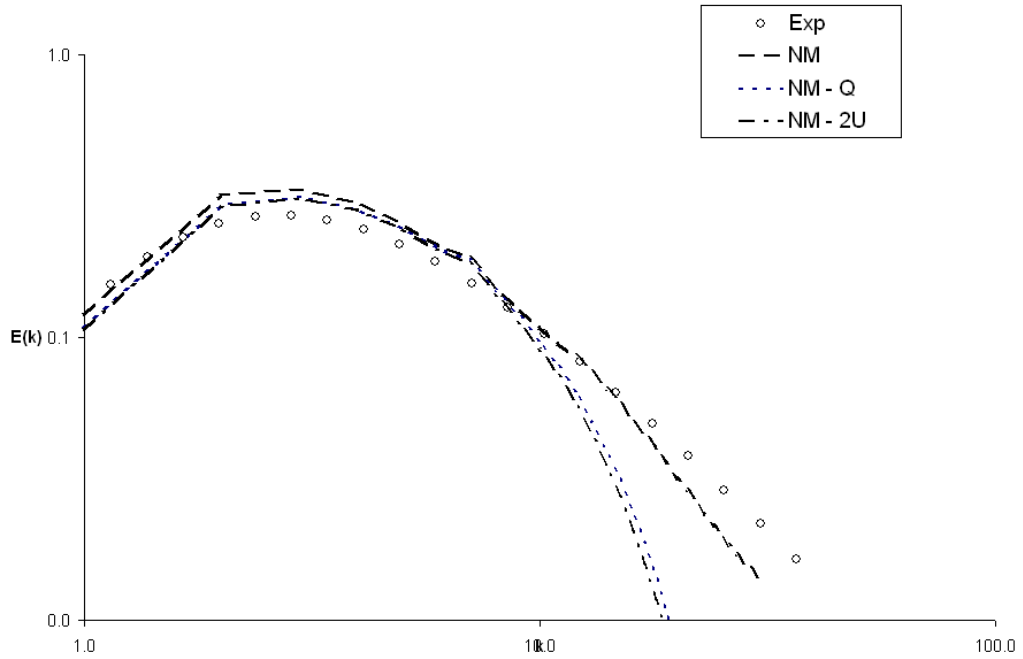
Figure 5.9

See appendix for details

45

5.3 Finite-Volume Simulation Results

Finite-volume simulation results showed similar behavior to the pseudospectral simulations, including the dissipative nature of the upwind biased schemes and the addition of energy in the high wavenumbers when using the central difference scheme. The decay of turbulent kinetic energy is shown for the Smagorinsky model, dynamic model, and MILES cases in Figures 5.10-5.12, respectively. In each case, the relative dissipation of the different numerical schemes is apparent (note that BCD and 1U refer to the bounded central difference and 1st order upwind schemes).
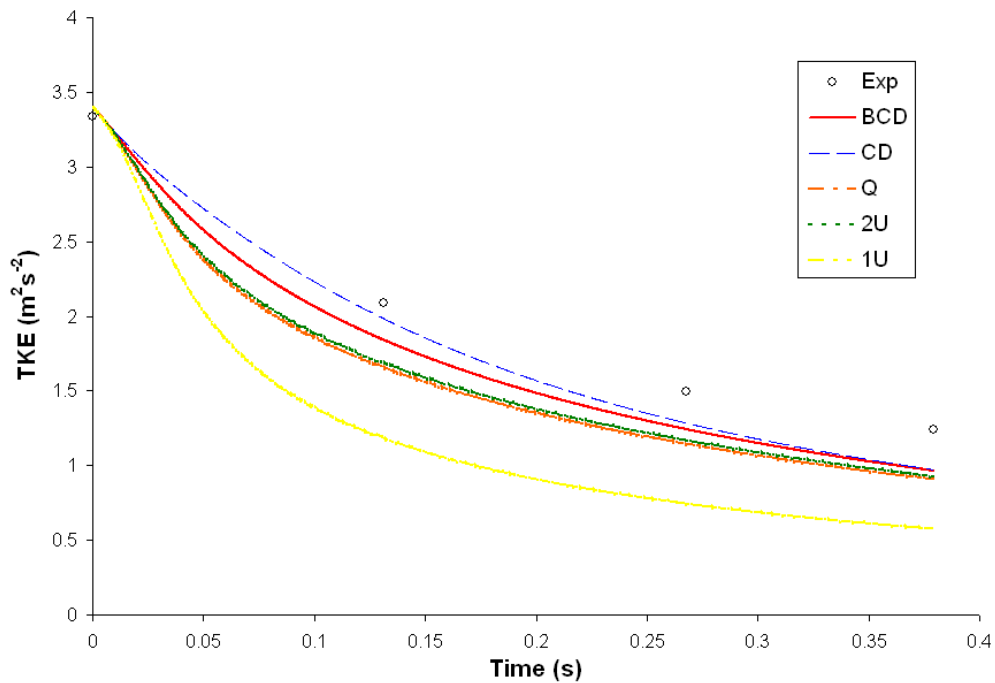
Figure 5.10

See appendix for details
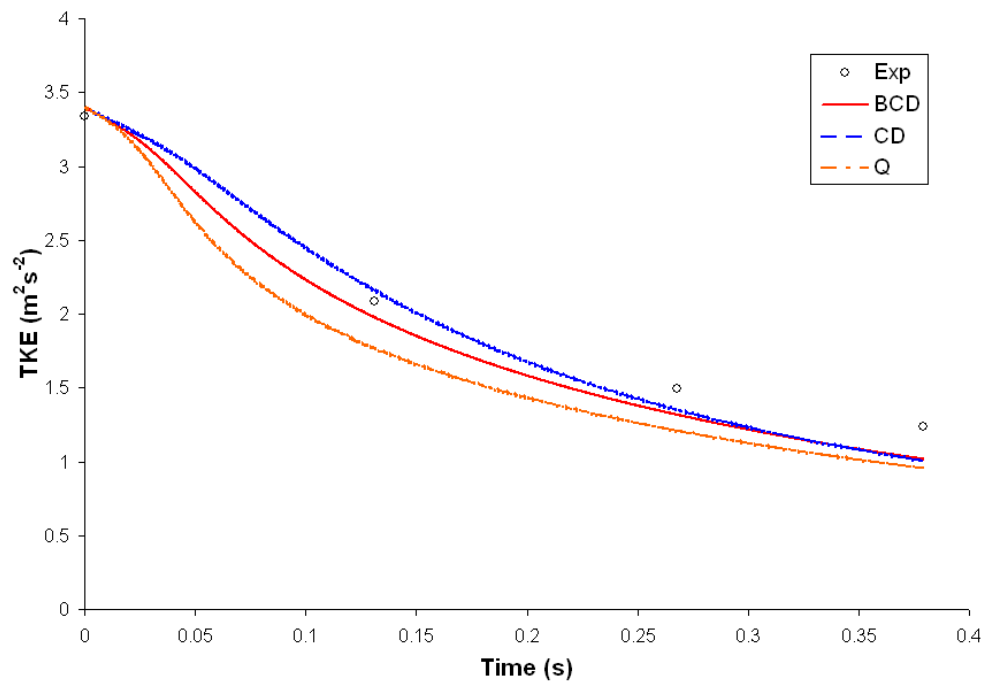
Figure 5.11

See appendix for details
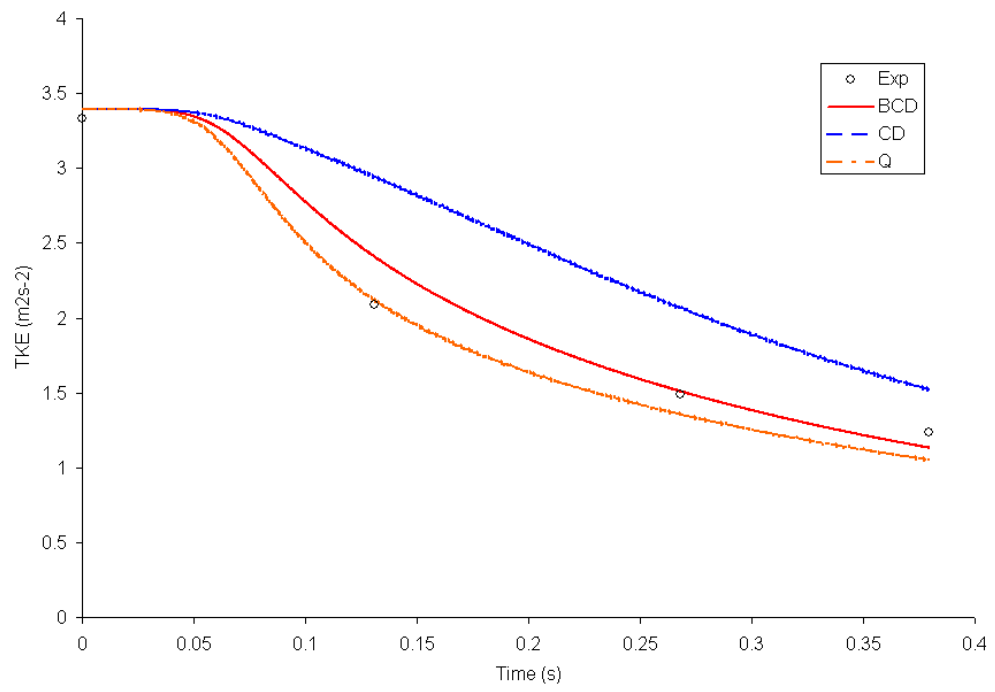
Figure 5.12

See appendix for details

Evaluation of the decay rates is complicated by the presence of an initial transient behavior in the results in which the initially random velocity modes organize into coherent structures with interscale dynamical behavior indicative of turbulent flow. Regardless, it is apparent that some combinations are either far too dissipative (SM-1U) or not nearly dissipative enough (MILES-CD). Note that, as with the pseudospectral simulations, both of the upwind biased second order schemes (2U and Q) show very similar behavior.
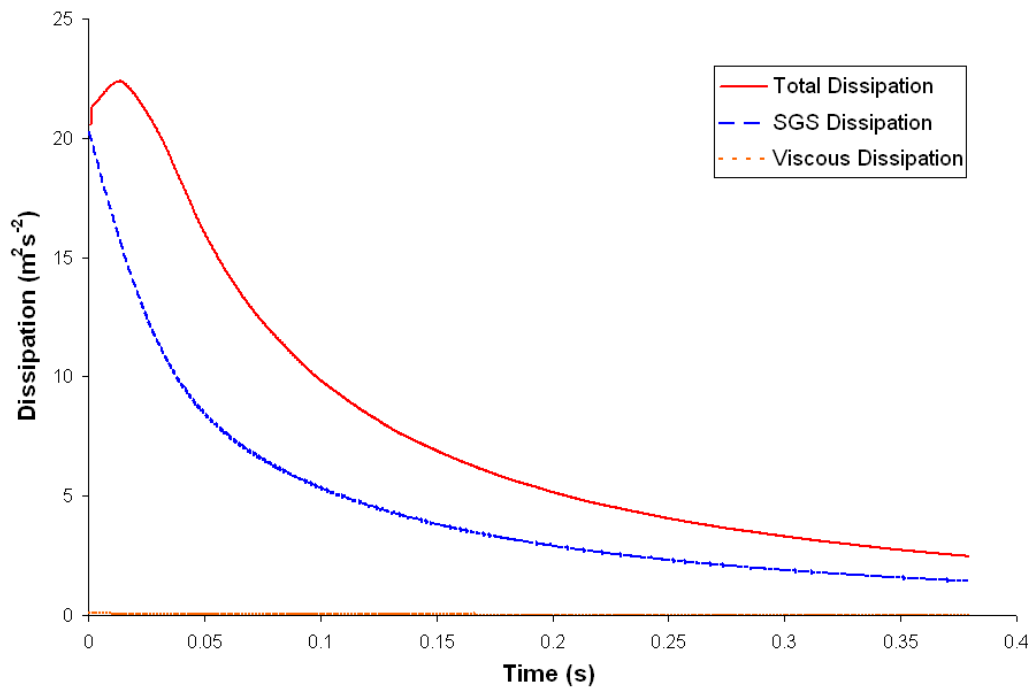
Figure 5.13

See appendix for details

Figure 5.13 shows the estimated contribution of the different dissipation mechanisms in the simulation with the Smagorinsky model and the bounded central difference scheme.

The total dissipation was estimated based on the time derivative of turbulent kinetic energy at each time step, and the SGS and viscous dissipation were estimated based on their volume averages. It is apparent that initially the dissipation is due almost entirely to the SGS model, but as the simulation proceeds a nearly constant ratio of SGS to total dissipation develops. The contribution of viscous dissipation is negligible for this high-Reynolds-number case.
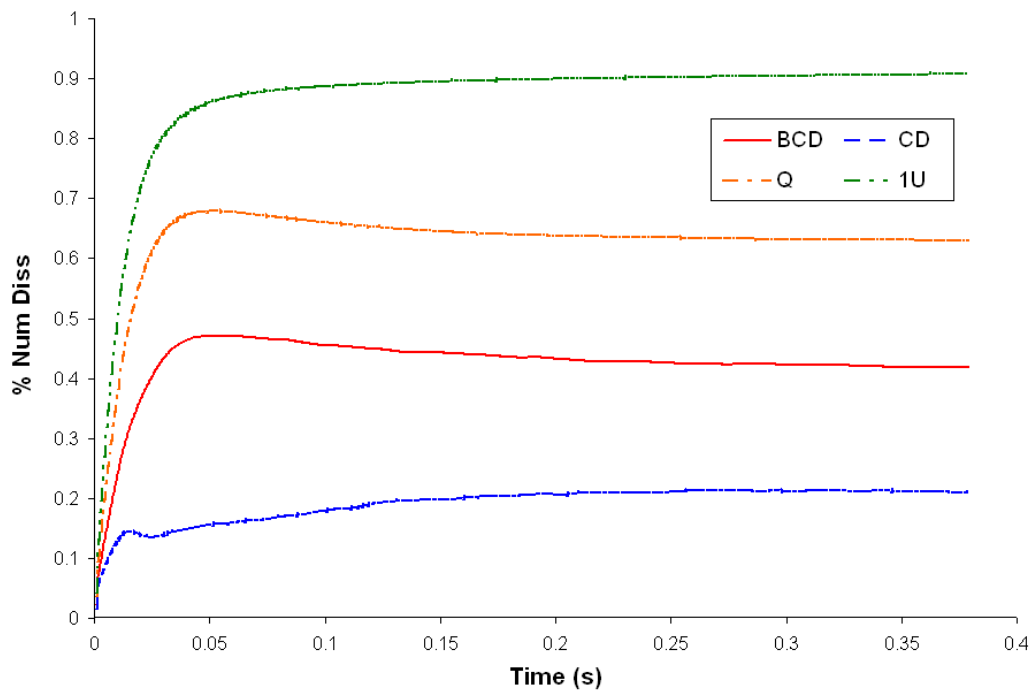
Figure 5.14

See appendix for details

The relative contribution of the numerical error for four of the schemes and the Smagorinsky model is shown in Figure 5.14. Not surprisingly, the more dissipative the scheme, the

50

higher the percentage of numerical dissipation. What is most relevant is the fact that two of the schemes, CD and BCD, have a larger contribution of the SGS stress than the numerical error, suggesting that these schemes may in general allow realistic results to be obtained with finite-volume LES. This observation is consistent with the assertion of Park et al. [23].

Energy spectra corresponding to the downstream-most measurement station are shown in Figures 5.15-5.16 for the Smagorinsky and dynamic Smagorinsky simulations. The Smagorinsky and dynamic results are similar and show good agreement with experiments for the low wavenumbers when using either the BCD or CD schemes. Results with the 2U, Q, and 1U schemes show too much dissipation, as expected.

Figure 5.17 shows the energy spectra obtained using the MILES approach and the various discretization schemes. The MILES results show good agreement with experiments when using either the BCD or Q schemes, although there is a slight overprediction of the energy in the lower wavenumbers. The MILES-Q result is arguably as good as the DSM-BCD result in terms of energy spectrum, although its formulation is much simpler in terms of both numerical method and SGS model. Interestingly, the MILES-BCD results shows the best agreement with experiments for the entire energy spectrum. The MILES-CD result, not surprisingly, is nonphysical.

The results suggest that a combination of CD or BCD scheme with either a Smagorinsky model or dynamic model may be sufficiently accurate for engineering simulations, with the BCD perhaps showing superior performance since there is no nonphysical pileup of energy in the high wavenumbers. All cases of SGS models with QUICK or second

51
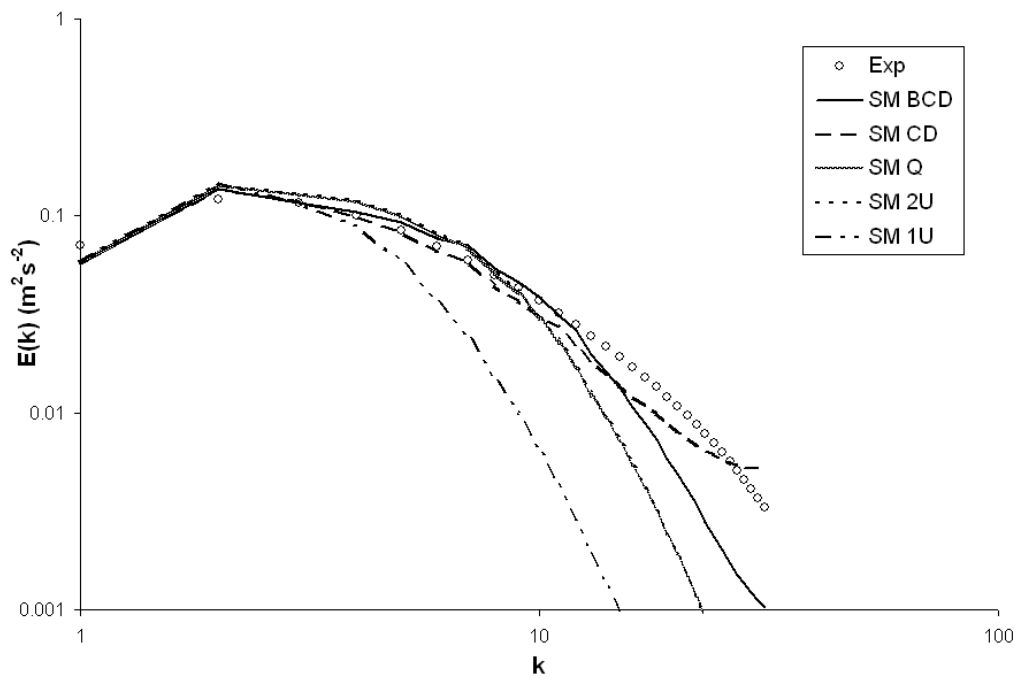
Figure 5.15

See appendix for details
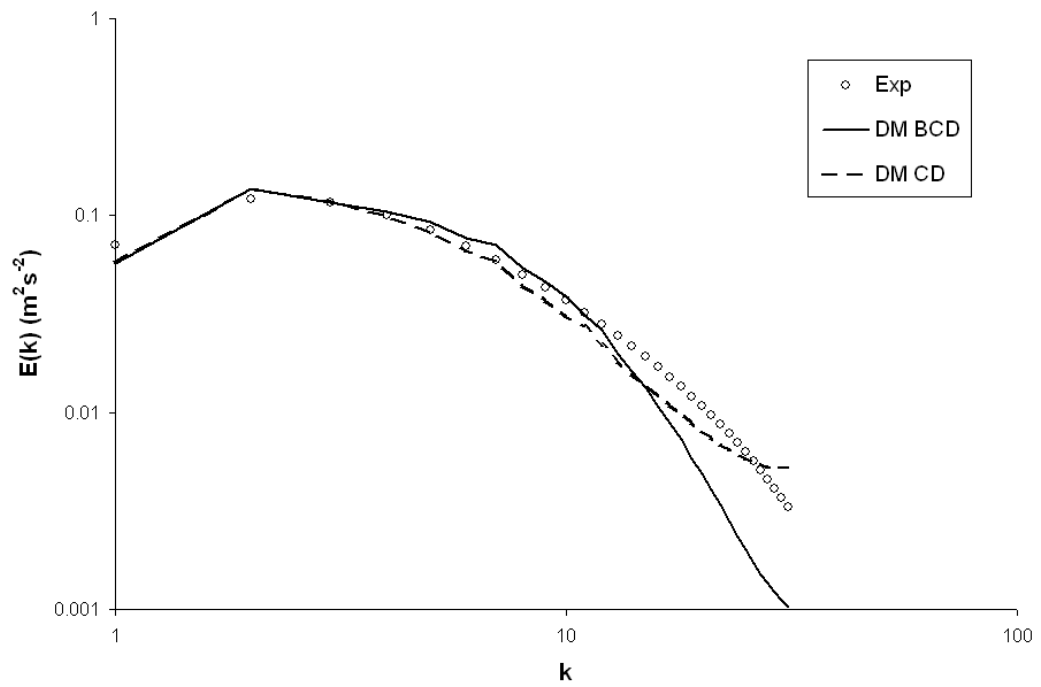
Figure 5.16

See appendix for details
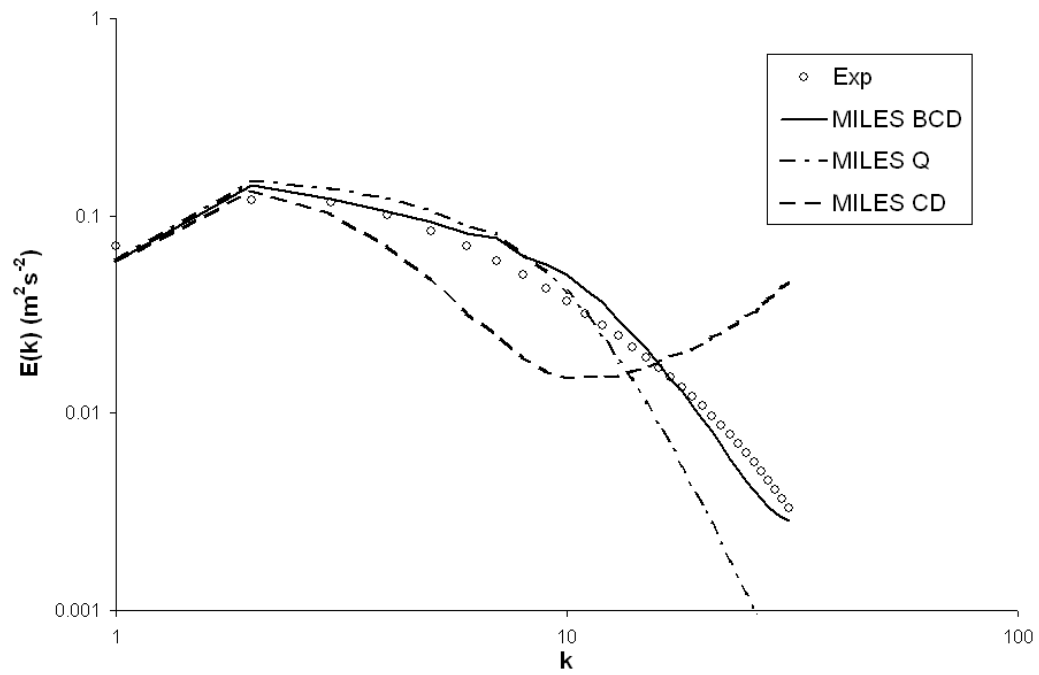
Figure 5.17

See appendix for details

order upwind show similar trends, and indicate that this combination is least desired since it tends to be overly dissipative. The results also suggest that a combination of BCD, QUICK or 2U scheme with the MILES approach may be sufficiently accurate for engineering problems.
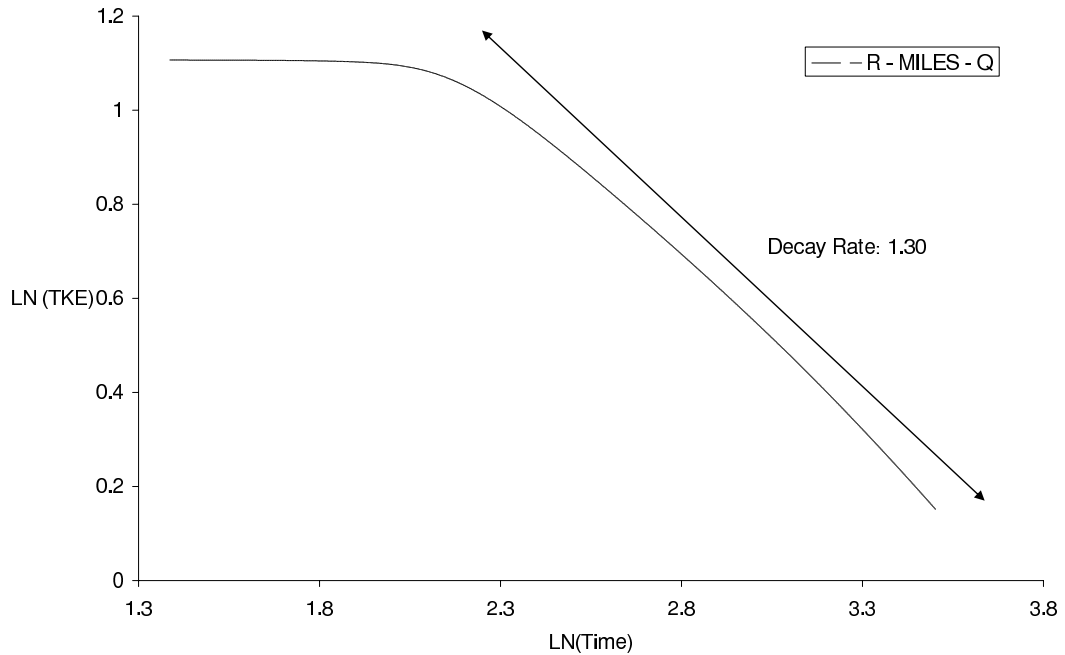
Figure 5.18

See appendix for details

Finally, the global combined influence of dissipative and dispersive effects due to SGS model and numerical scheme can be quantified based on the power law decay rate. Turbulent kinetic energy is traditionally to follow a (temporal) decay at high Re of the form:

$$k = k_o \left(\frac{t}{t_o} \right)^{-n} \tag{5.1}$$

55

Values of the decay exponent n reported in the literature lie between 1.15 and 1.45 [24], but Mohamed and LaRue [19] assert that $n = 1.3$ best collapses all available data. For the current the case, Kang et al. [15] report the decay exponent to by $n = 1.25$. In an attempt to evaluate the decay rates to a reasonable degree of accuracy, the numerical simulation was initialized with a velocity field whose phases are assumed to have adjusted to appropriate values and then rescaled to the correct filtered energy spectrum. Figure 5.18 shows the filtered kinetic energy as a function of time on a logarithmic scale for the MILES with QUICK numerical scheme. The region of interest is the locally linear region at the later times. $Table$ 5.1 shows the calculated decay coefficient for several combinations of SGS models and numerical schemes. The decay coefficients for MILES with QUICK and for Smagorinsky with QUICK and 2U give the closest results to the experiments. The SM-BCD results lies at the upper limit of reported values while all others (except for the case with 1st order discretization) overpredict decay rate significantly. Interestingly, the MILES-BCD combination, which showed the best energy spectrum, shows the worst prediction of decay rates.

Table 5.1

See appendix for details

	MILES	DSM	SM
BCD	1.81	1.68	1.46
CD		1.78	1.66
$QUICK$	1.29	1.38	1.23
$2U$			1.32
$1U$			0.93

CHAPTER 6

ENGINEERING APPLICATION: ROUND JET FLOW

6.1 Brief

The axisymmetric jet experiment of Hussein et al. [14] serves as an application problem used to verify the behavior documented in earlier sections of different combinations of SGS model and discretization schemes for use in large eddy simulation of turbulent flow. The motivation of the experimental work [14] was to determine the source of discrepancy in high velocity data from previous axisymmetric jet flow experiments. One source of discrepancy was found to be a result of enclosure. Therefore, Hussein et al. [14] ensured that the experimental facility was large enough to be considered as an infinite environment. Also, the paper validated burst mode laser dopper anemometer (LDA) and flying hot wire data (FHW) data by showing that the results obtained together with the governing equations and boundary conditions for the axisymmetric jet were satisfied.

6.2 Simulation Setup

The experimental setup of Hussein et al. [14] served as a guide for performing large eddy simulation of a high-Reynolds-number ($Re = 10^5$) turbulent jet simulation. The experiment was performed in an environment large enough to be approximated as infinite

comparable to the span of the jet exit diameter, $D = 1in$. In this way, disturbances due to entrained recirculation flow were avoided.

Wall

Pressure Inlet

Velocity Inlet
D = 1 inch

5D

3D

Pressure Inlet

Pressure Outlet

60D

115D
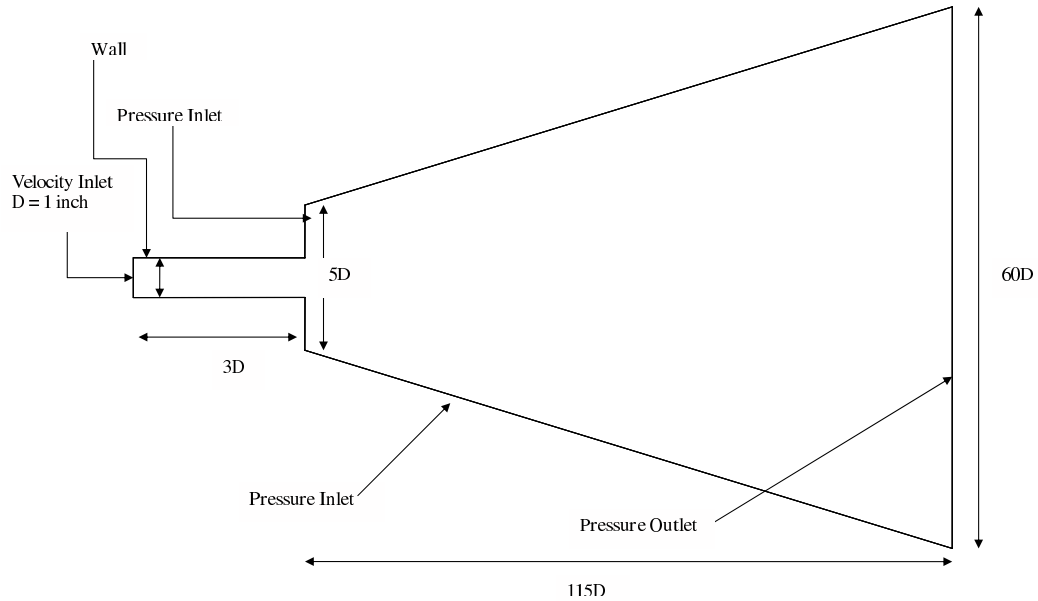
Figure 6.1

See appendix for details

With this requirement in mind, the computational domain as shown in Figure 6.1 was built with a diameter 5 times larger than the jet exit diameter at the jet exit and growing at a rate of 0.5 inches per inch in the streamwise direction. The maximum streamwise domain extent was $115D$ downstream of the jet exit with a maximum outer diameter of 120D. The domain size was estimated to be sufficiently large to completely contain all of the jet mixing behavior, and this was subsequently borne out by the results.

Figure 6.1 also shows the boundary conditions specified in the flow solver. A uniform velocity was applied at the jet inlet as indicated. All of the outer boundary external to the

jet was specified as constant (ambient) pressure. This choice of boundary condition allows low velocity entrainment of ambient fluid into the jet and most accurately reproduces the effects of an infinite domain.

From [14], the jet exit velocity was found to follow close to a top-hat profile with a laminar boundary layer thickness of $\delta_{95} = 0.7mm$ close to the jet lip. In the numerical experiment, a boundary layer thickness of $\delta_{95} = 0.7mm$ was achieved by including an inlet supply pipe as shown. The length of the supply pipe was estimated by solving the flat plate laminar boundary layer equation for the x distance needed. The flat plate boundary layer equation yields:

$$\frac{\delta}{x} = \frac{5}{Re^{\frac{1}{2}}} \tag{6.1}$$

where Re is the Reynolds number equal to:

$$Re = \frac{Ux}{\nu} \tag{6.2}$$

Given the experimentally determined jet exit velocity $U = 56.2m/s$, the above equation may be solved to find the x distance:

$$x = 2.9134 inches \tag{6.3}$$

From this, a distance of 3 inches was determined to be the sufficient pipe length required to allow for a boundary layer thickness of $\delta_{95} = 0.7mm$ at the jet lip. Figure 6.2 shows a closeup view of the mesh around the pipe inlet. Closer to the wall the cells were designed to be of a higher density. In that way that the boundary layer was accurately resolved. The timestep size used in the simulations was determined by computing the time required for a fluid particle traveling at the jet exit velocity to traverse one grid cell, based on the smallest

streamwise extent in the mesh. This corresponds to a maximum (convective) CFL number of one. The time step size was determined to be $\Delta t \approx 1E - 6$.
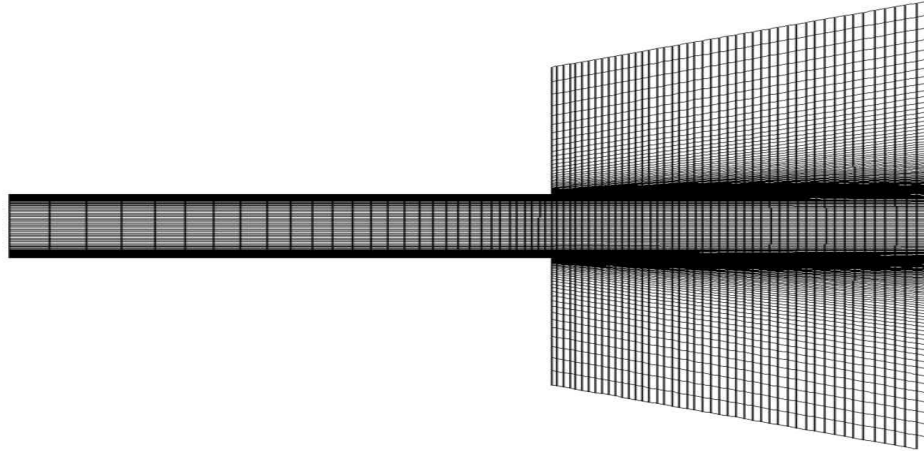
Figure 6.2

See appendix for details

Figure 6.3 shows a plan view of an isosurface cutting plane through the computational domain. The domain was made up of approximately three million grid cells. From the jet inlet as shown on Figure 6.3 to the pressure outlet region, the domain was constructed with 345 nodal points. Figure 6.4 shows the axial, radial and azimuthal distribution of grid points which are in constant ratio throughout the domain. The computational domain was constructed in such a way that 100 points lie in the radial direction from the center of Figure 6.4 to the outer edge.
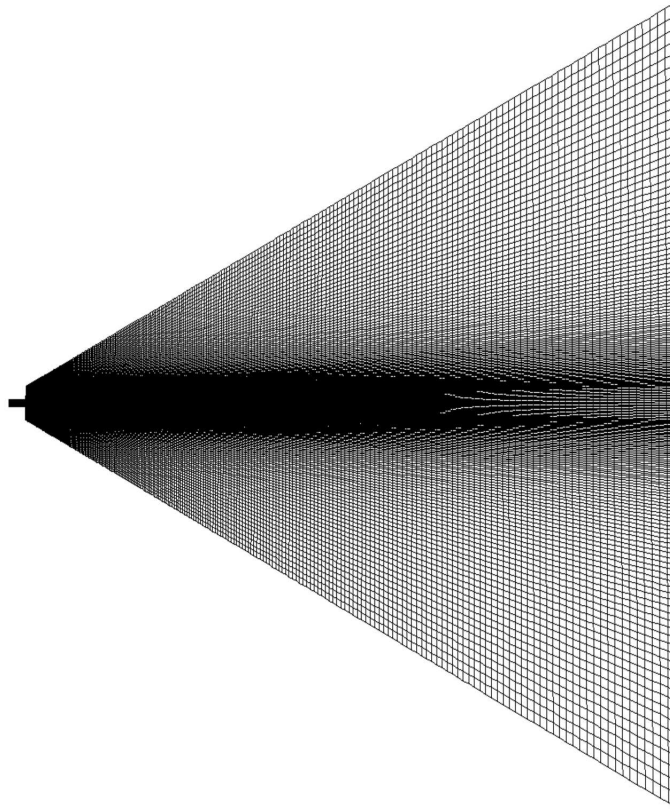
Figure 6.3

See appendix for details
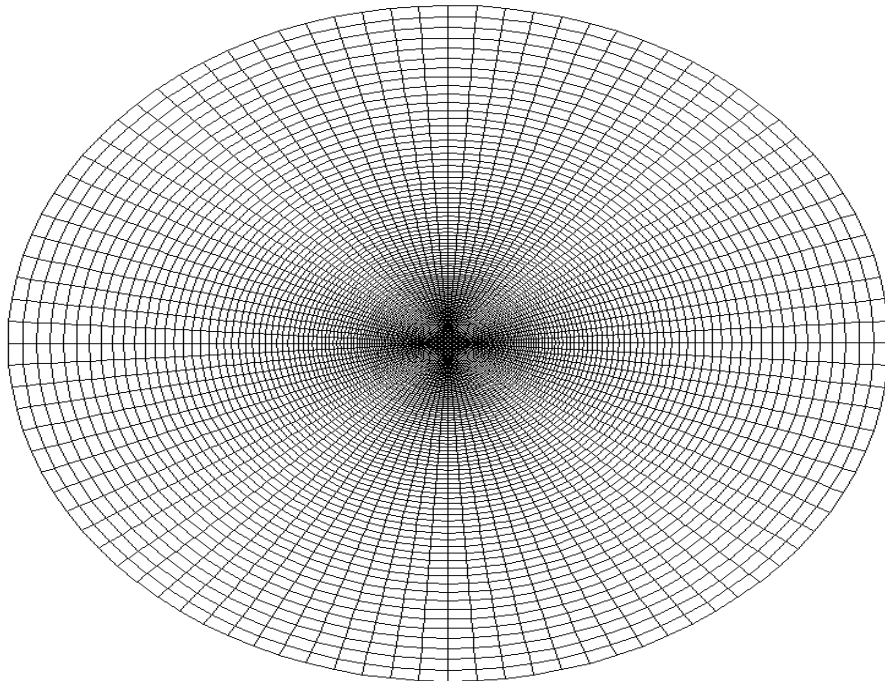
Figure 6.4

See appendix for details

6.3 Results

In an attempt to test the conclusions made in earlier chapters on favorable combinations of SGS models and discretization schemes, large eddy simulation of a high-Reynolds-number, momentum conserving, axisymmetric turbulent jet at Mach number 0.2 was performed. The combinations simulated were Smagorinsky and dynamic Smagorinsky with bounded central differencing (SM-BCD, DSM-BCD) and monotonically integrated large eddy simulation with second order upwind scheme (MILES-2U). Numerical simulations were constructed following the experimental setup of Hussein et al. [14]. Simulations were performed on 24 processors of a SGI ORIGIN 3800, 128 processors (400MHz R12000), 128 Gigabytes of RAM.

Figure 6.6 shows the convergence history for a combination of SM with BCD for the running-time-averaged streamwise velocity component at a position 10 diameters downstream of the jet exit. As expected, with a grid of approximately three million cells, a fully converged solution set requires an extensive amount of computational time, perhaps on the order of one month. Common to all of the round jet simulations performed, the maximum number of timesteps attained per day was approximately one thousand. After 40000 iterations the simulations were determined to have converged to a reasonable degree, though for DSM-BCD the simulation was judged converged at a number of iterations closer to 50000.

An illustration of the instantaneous streamwise velocity distribution in the jet is shown in Figure 6.5. The contours highlight the fundamental aspect of LES, namely that the large turbulent flow structures are resolved in the simulation. Also apparent in the Figure
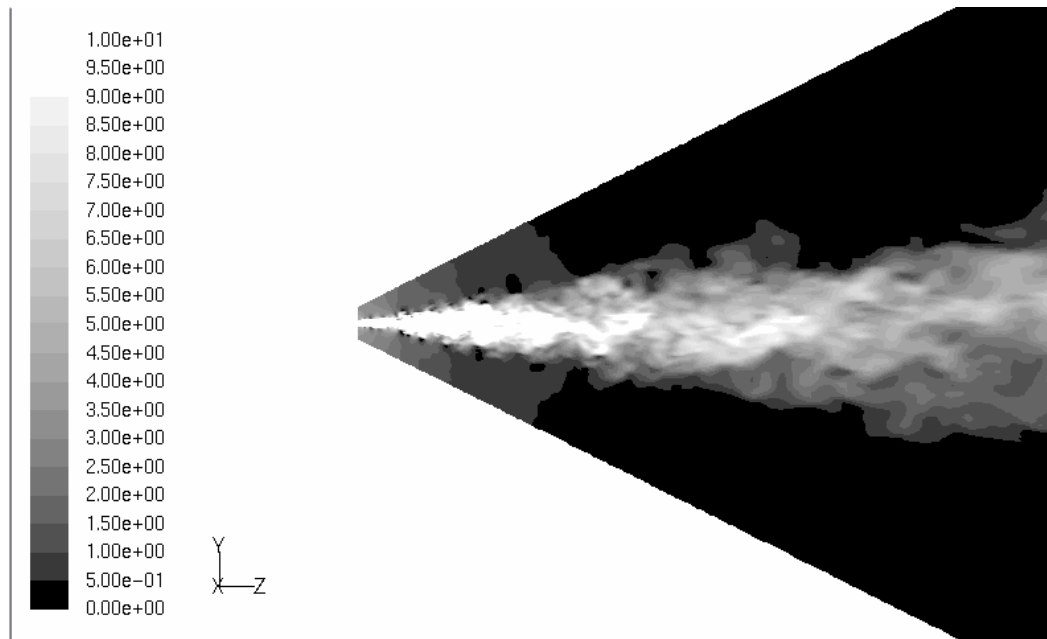
Figure 6.5

See appendix for details

is the entrainment of ambient fluid into the jet, made possible by the use of pressure inlet boundary conditions.

Figure 6.7 shows a plot of the inverse of centerline velocity versus downstream distance for each of the combinations of SGS model and numerical discretization scheme plotted with the stationary hotwire data of Hussein at al. [14]. The virtual origin for all the simulations was determined to be within $4.9D \pm 0.6D$, upstream of the jet exit. As shown, the decay rate for the MILES-2U case compares very well with experimental data while the SM-BCD and DSM-BCD cases underpredict the rate of decay of the normalized centerline velocity. Similar to the findings of [14], a locally linear region exists between 40D and 100D which implies that the jet spreading rate is approximately locally constant
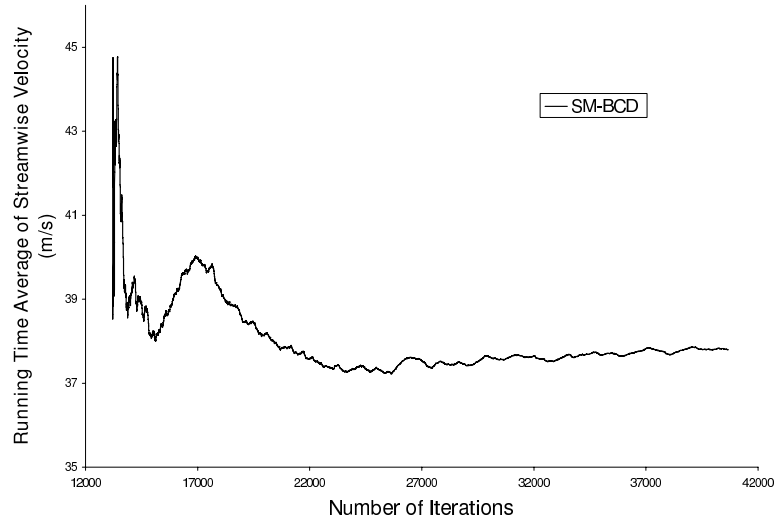
Figure 6.6

See appendix for details

at positions far from the jet exit. Therefore data was collected from the simulations at several positions downstream of the jet exit: at 50D, 70D and 90D.

Figure 6.8-6.10 shows the running-time-averaged normalized streamwise velocity versus the nondimentional radial distance $\eta = \frac{r}{x-x_o}$ at the three downstream positions. All combinations of SGS model and discretization scheme are in good agreement with experimental data. The normalized simulation results show little dependency on downstream position (x/D) indicating a self similar profile in the region from 50D through 90D.

Second order moments of velocity are plotted in Figures 6.11-6.19 at several downstream locations. Figure 6.11-6.13 shows a plot of the axial component of the Reynolds stress term non-dimensionalized by the square of centerline velocity versus non-dimensionalized radial distance η. The result emphasizes self similarity further downstream. All cases un-

65
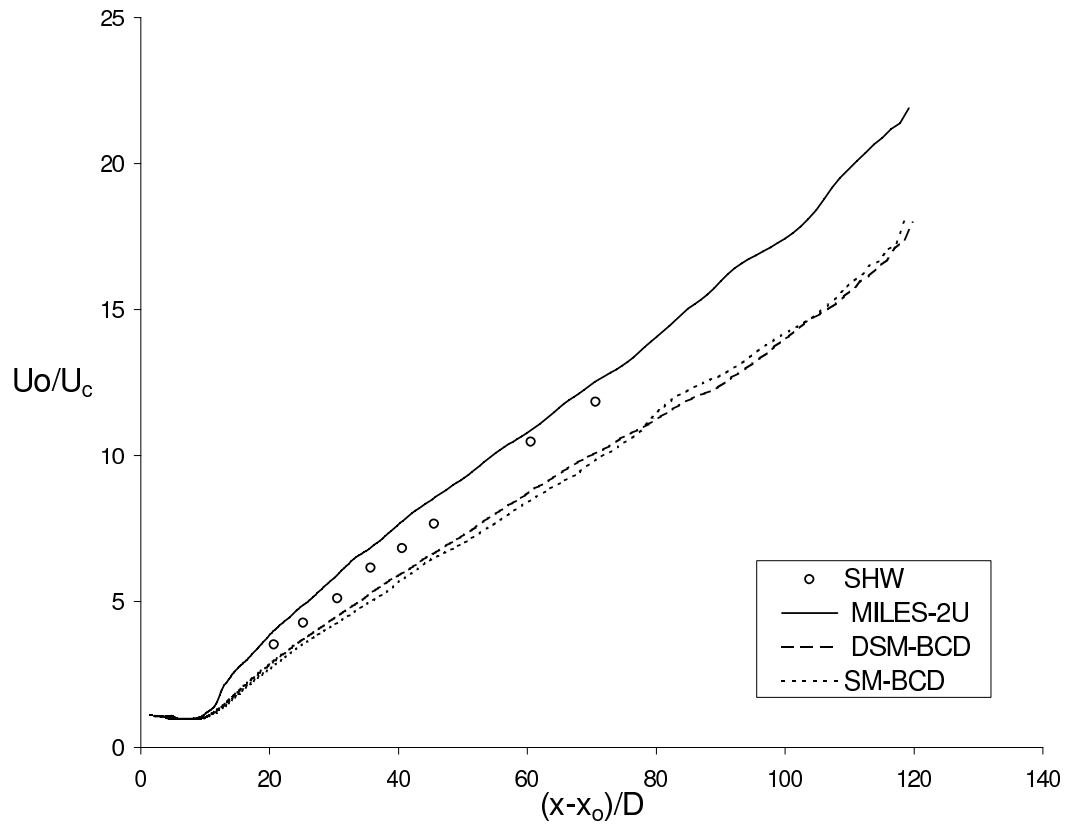
Figure 6.7

See appendix for details

66
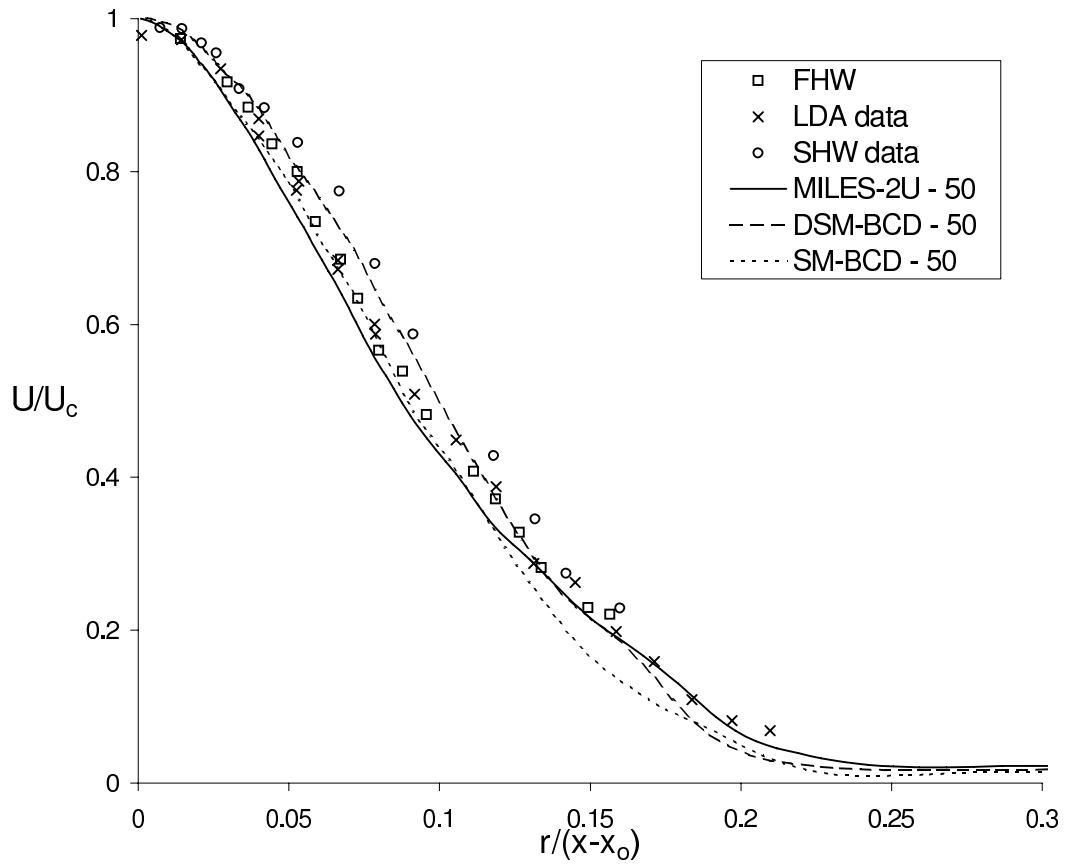
Figure 6.8

See appendix for details
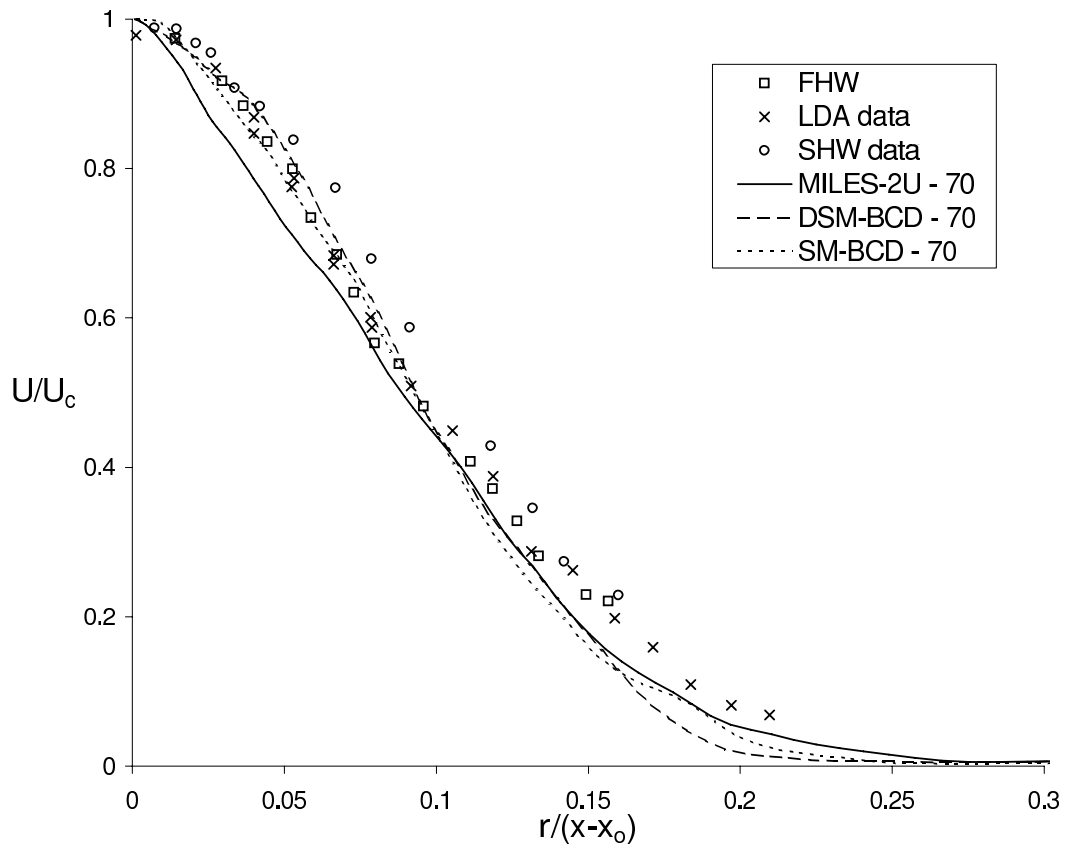
Figure 6.9

See appendix for details
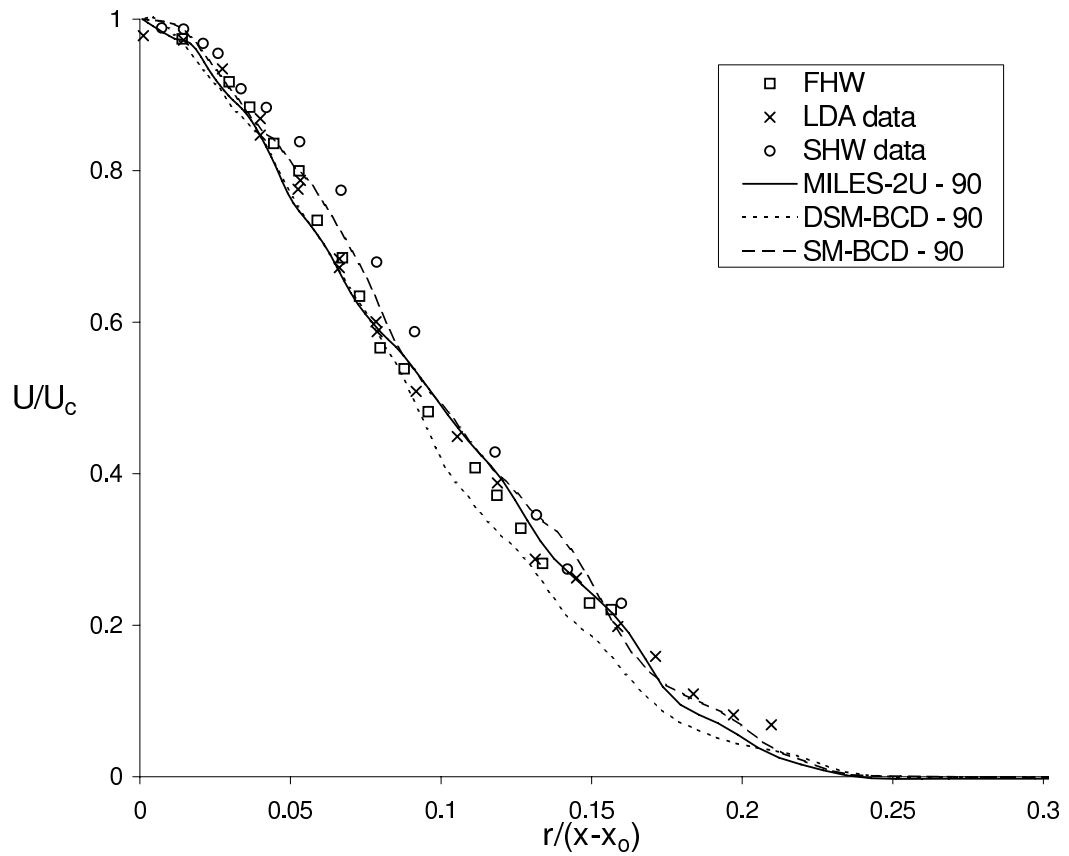
Figure 6.10

See appendix for details

derpredict the experimental data on average, but the MILES-2U case seems to do it the

least.
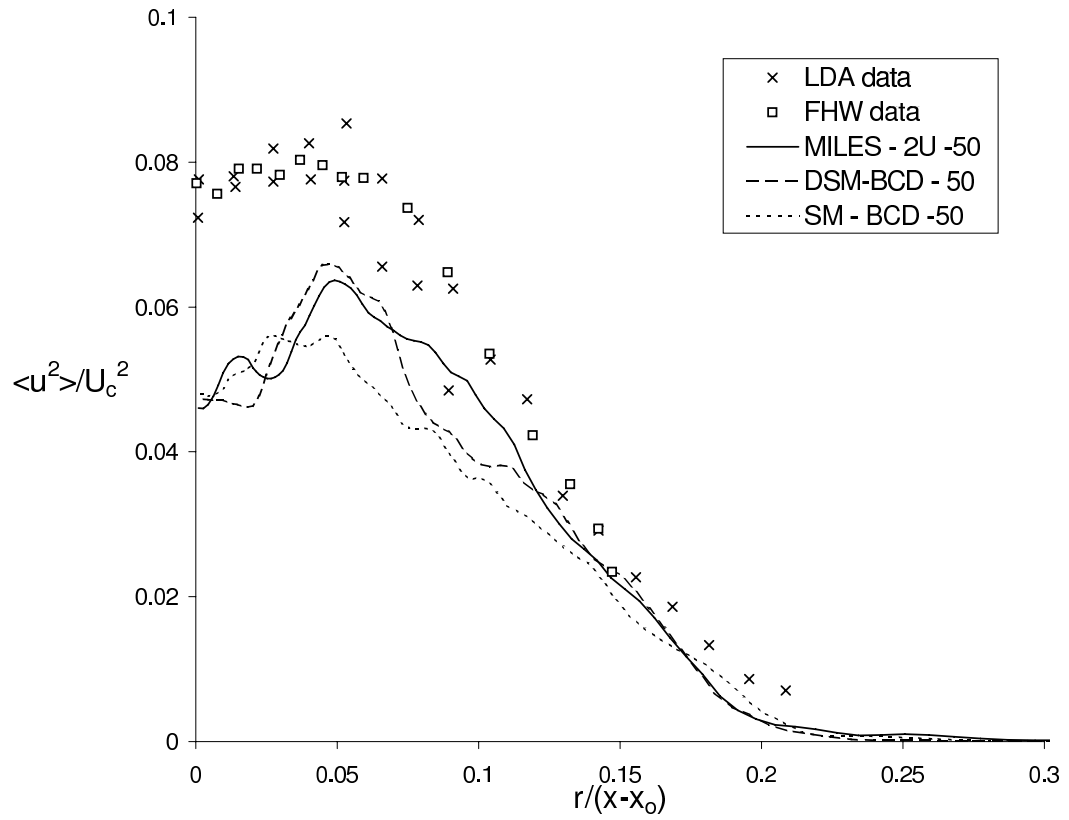
Figure 6.11

See appendix for details
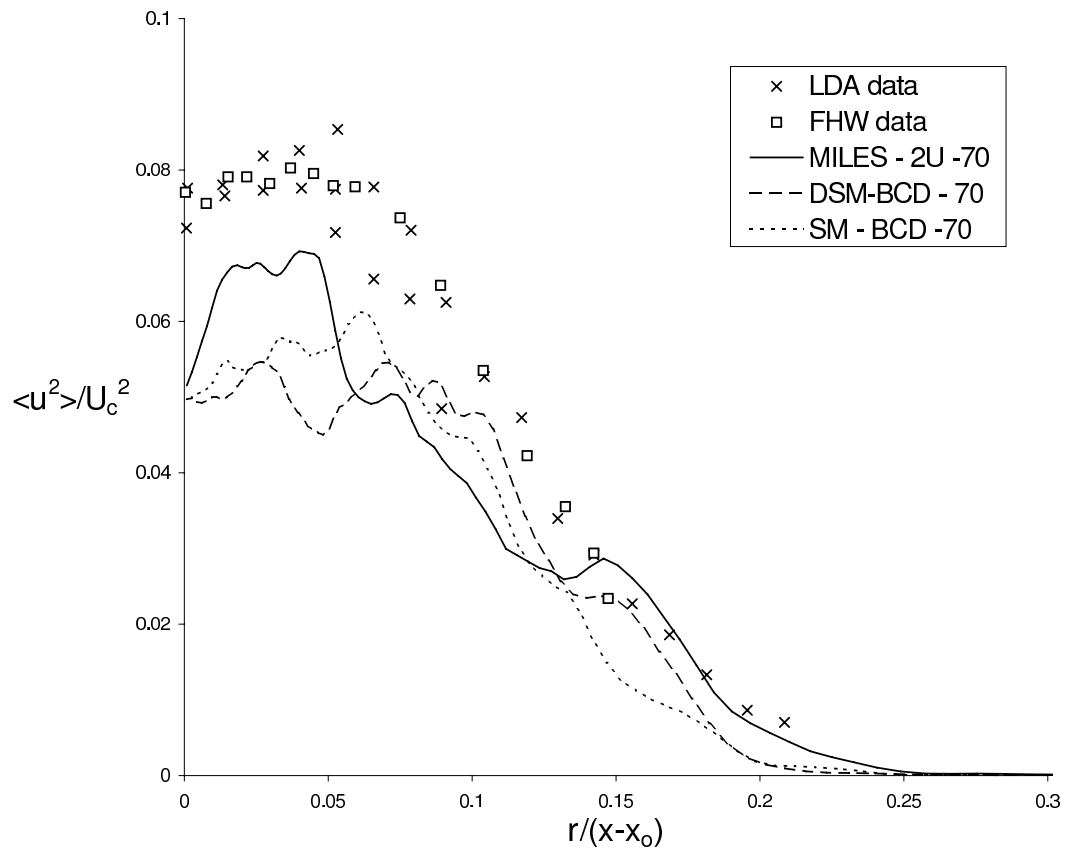
Figure 6.12

See appendix for details
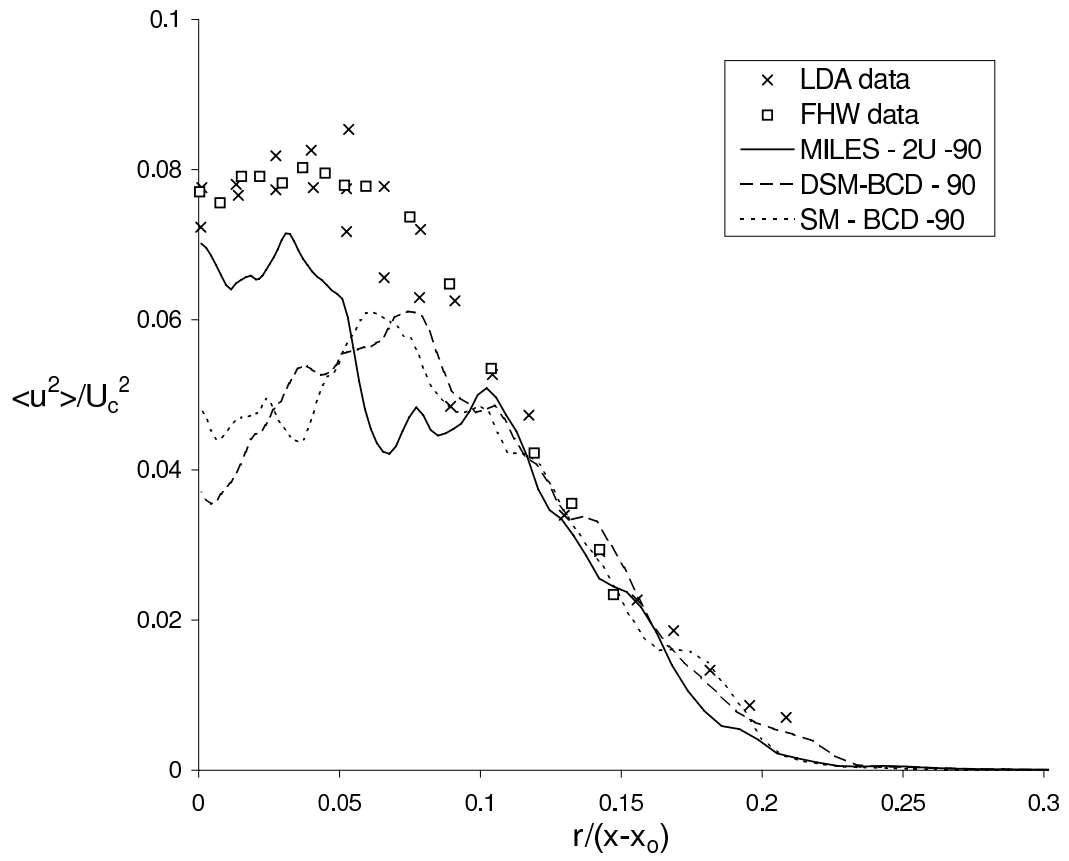
Figure 6.13

See appendix for details

73
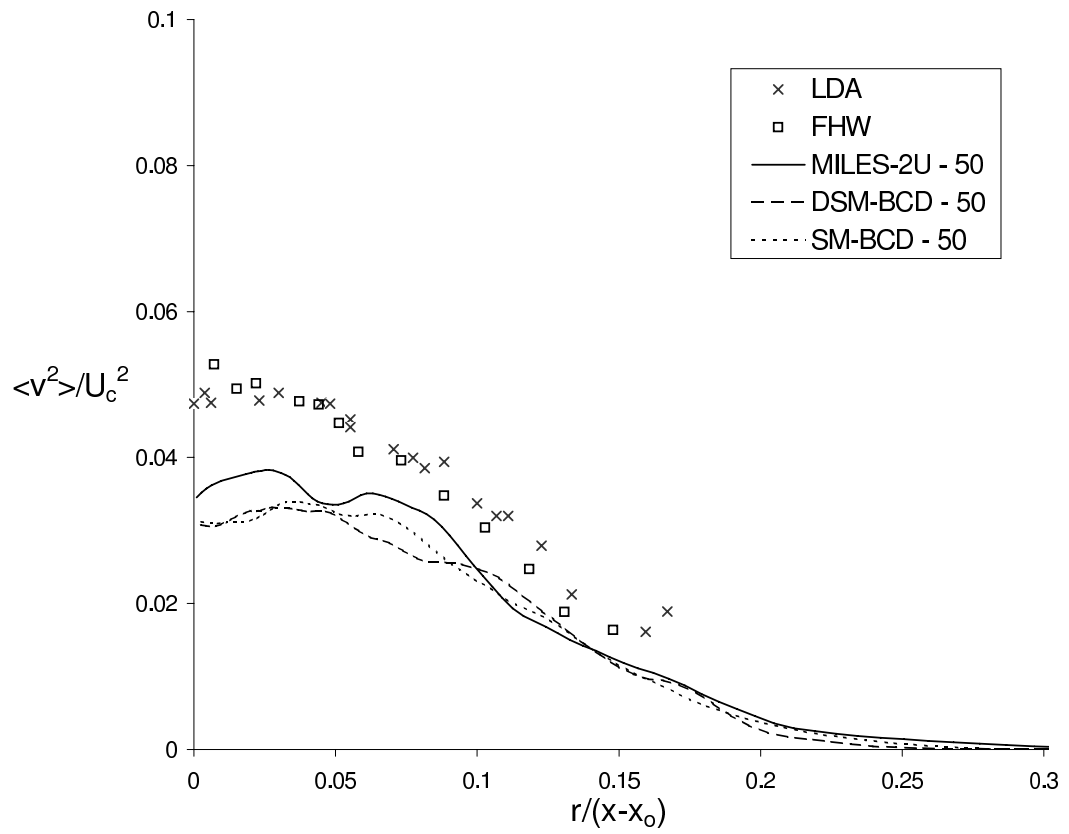
Figure 6.14

See appendix for details
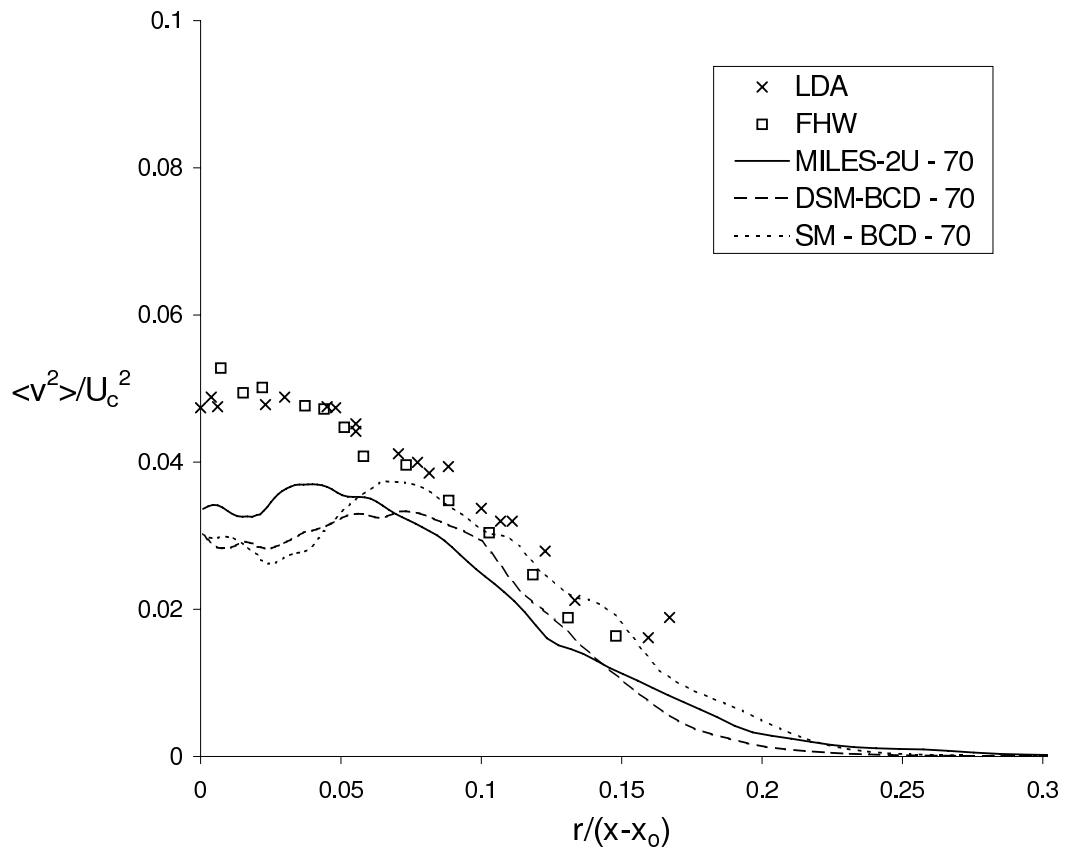
Figure 6.15

See appendix for details
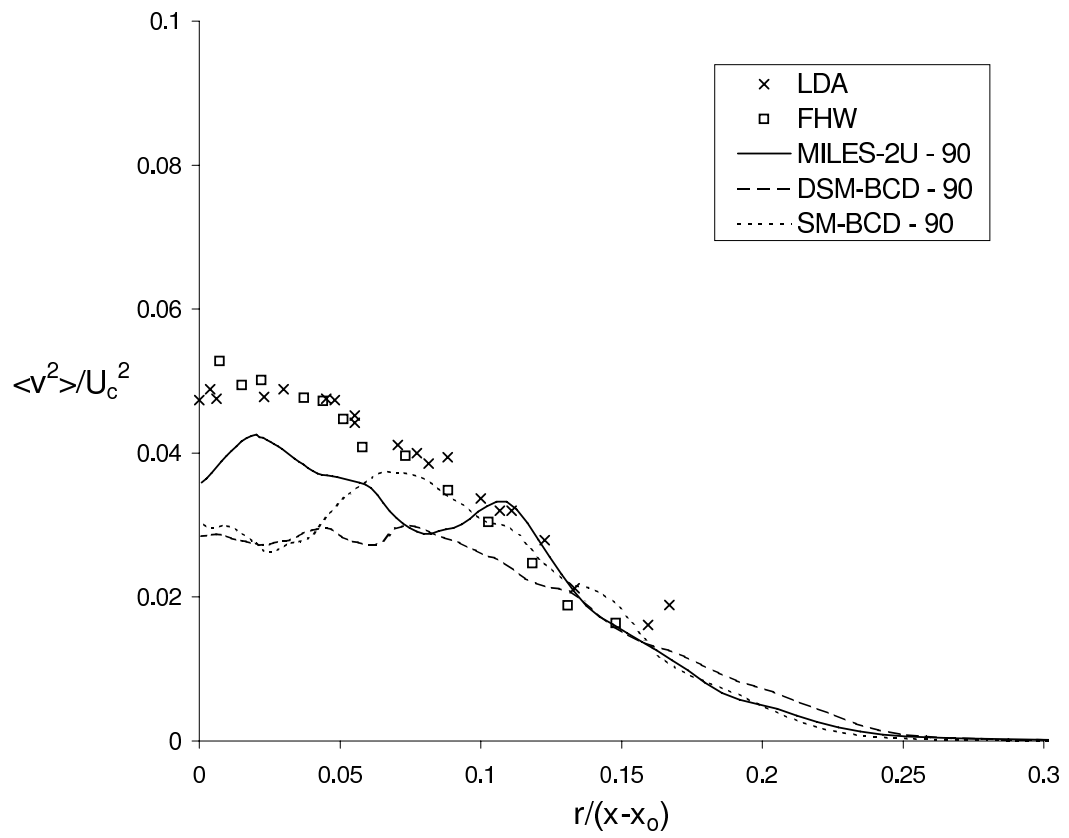
Figure 6.16

See appendix for details
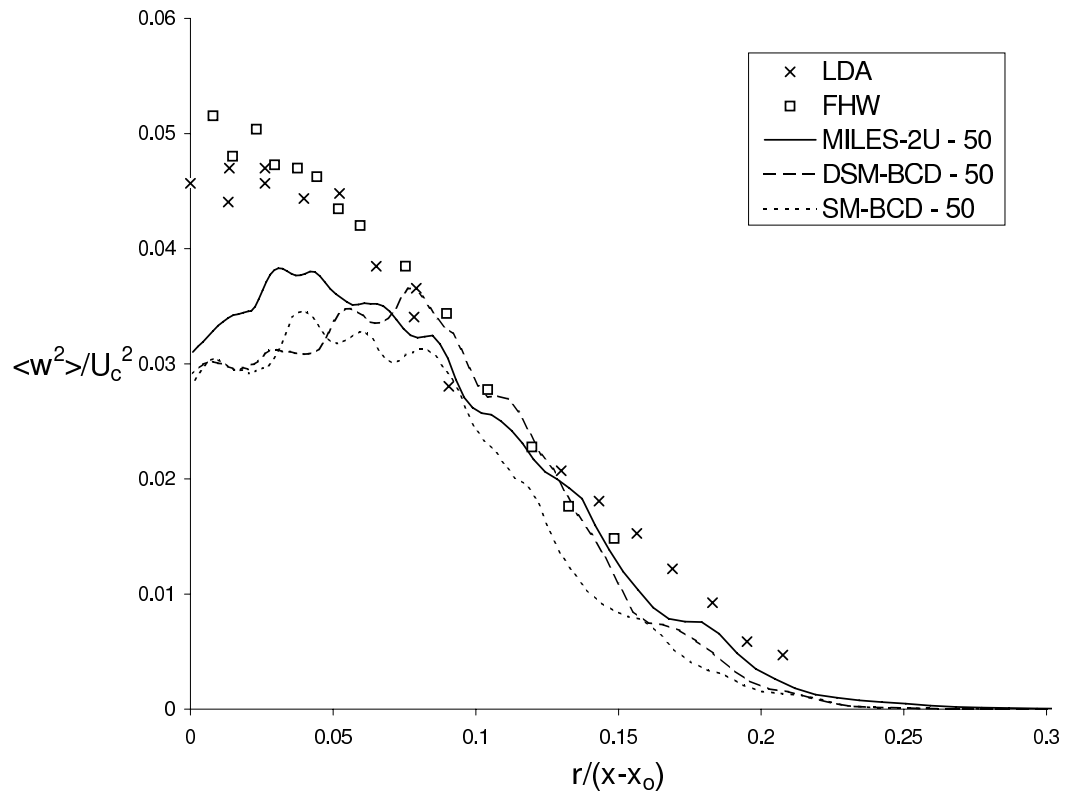
Figure 6.17

See appendix for details
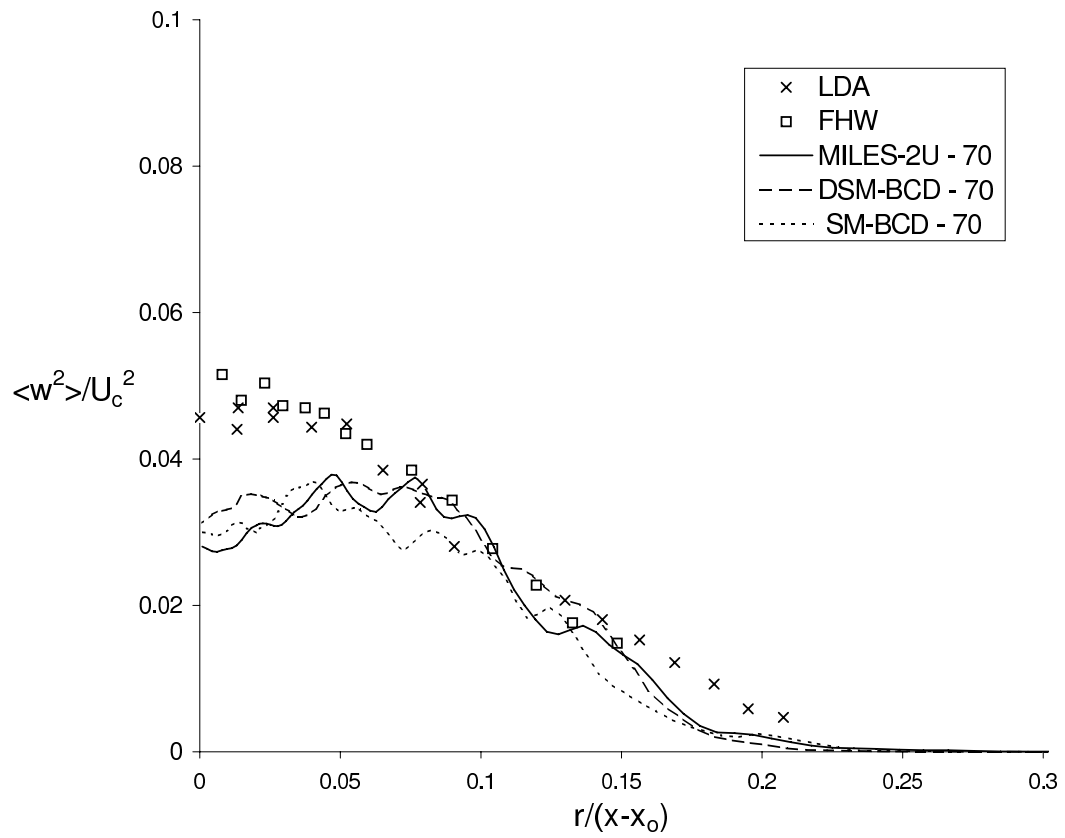
Figure 6.18

See appendix for details
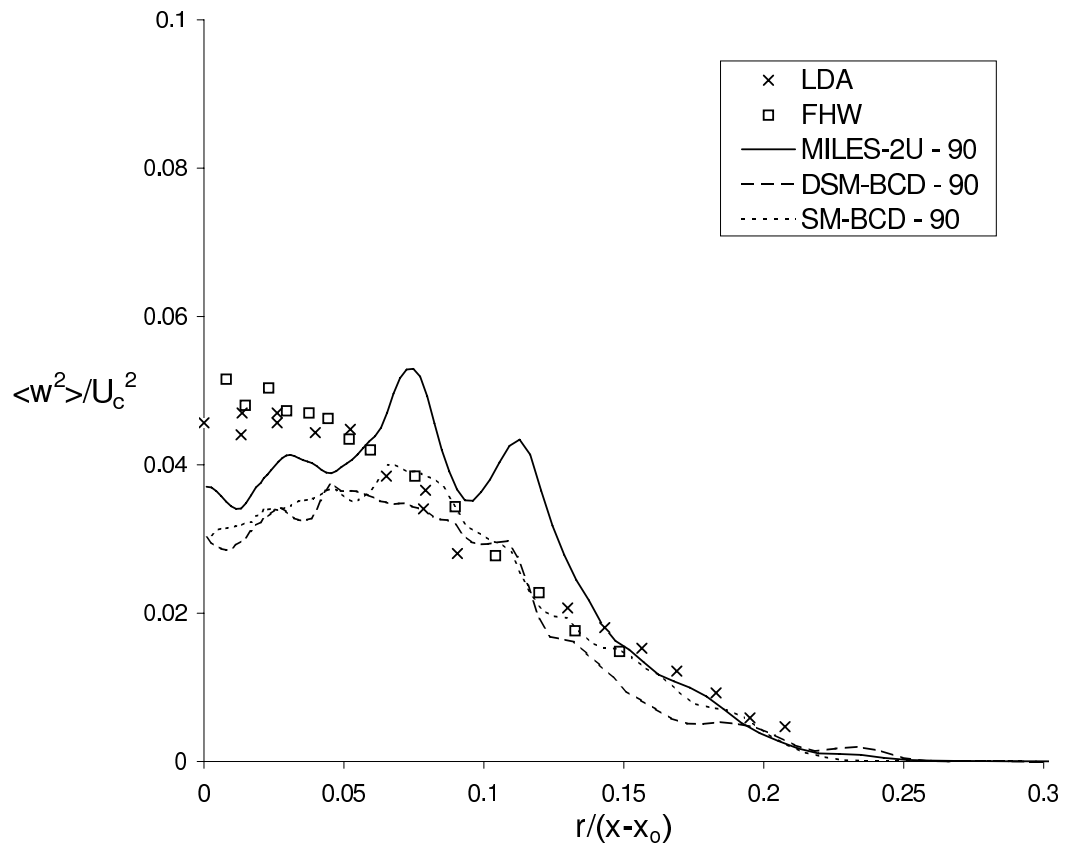
Figure 6.19

See appendix for details

CHAPTER 7

CONCLUSIONS

The goal of this research effort was to determine optimum combinations of closure model and discretization schemes for use in performing LES in complex engineering environments using readily available CFD flow solvers. The investigation proceeded in two parts. A formal quantification of discretization error present in finite-volume/finite-difference simulations was conducted. The effect of these errors was then explicitly incorporated into the pseudospectral LES solver and used to compute LES of decaying isotropic turbulence on both 32^3 and 64^3 grid resolutions. This was accomplished based on a truncated Taylor series representation of numerical error in physical space, transformed via the Fast Fourier Transforms to wavenumber space. To this author's knowledge, this is the first documented use of such an approach. Comparisons were made in terms of energy spectra at different downstream positions and used to characterize the influence of different SGS models and discretization schemes on the simulation.

Verification of results was carried out using a commercially available finite-volume/ finite-difference solver (FLUENT$^{\textregistered}$). The purpose of the finite volume simulations was to verify that the observations made using the modified psuedospectral code as a tool for determining favorable combinations of closure models with numerical schemes hold for simulations in physical space. Therefore the finite volume simulations were per-

formed with equivalent specification as those of the pseudospectral simulations. Numerical discretization schemes experimented with included second order Central Differencing (CD), QUICK (Q), Upwind (2U), Bounded Central differencing (BCD) and first order upwind (1U). Turbulence closure models implemented included Smagorinsky (SM), dynamic Smagorinsky (DSM) and Multiscale(MSM). Also implemented was the numerical LES technique Monotonically Integrated LES (MILES).

For the pseudospectral simulations, it was first necessary to determine the appropriate number of terms needed to be retained in the Taylor series expansion of the numerical error term. To do this, simulations were conducted using a successively larger number of terms to represent the numerical differentiation error. The result showed that after the third truncation error term there is no significant change in the computed energy density spectrum using the 2U, QUICK, and CD schemes.

The study proceeded by performing simulation of the aforementioned SGS models with discretization schemes. In general, the results from the pseudospectral simulation highlight the dissipative nature of the upwind biased schemes. The effect was most apparent at higher wavenumber where the results clearly indicate that there is an excessive removal of energy indicated by the underprediction of the experimental data. Similarly, the central differencing cases showed an excess dispersion and non-physical energy at high wavenumbers. The results showed that the eddy viscosity SGS models investigated (SM, DSM, MSM) added significant dissipation especially at higher wavenumbers. These suggested that an optimum combination of SGS model and discretization scheme should allow zero dispersion error (eliminating CD as a preferred scheme) and should provide an

adequate but not excessive level of dissipation, in order to correct representative energy transfer from the resolved to the unresolved scales of motion. This level of dissipation should be due to the combined effect of the numerical scheme and or the SGS model.

Finite-volume simulation results showed similar behavior to the pseudospectral simulations, including the dissipative nature of the upwind biased schemes and the addition of energy in the high wavenumbers when using the central difference scheme. In addition, the BCD scheme which combines the effect of a central differencing and an upwind scheme was investigated. Of the combinations investigated, those that seemed most likely to satisfy chacteristics suggested by the pseudospectral results were the BCD model with either the SM or DSM eddy viscosity model or the MILES method with either 2U or QUICK discretization scheme. These combinations should introduce zero dispersion error. Further, the BCD scheme provides (relatively) small numerical dissipation, so combining it with a dissipative eddy viscosity model might lead to an appropriate level of combined dissipation. Alternatively, the MILES method with the more dissipative QUICK or 2U scheme may provide sufficient dissipation through the discretization scheme alone. The energy spectra from the finite-volume simulations confirmed the behavior predicted by the pseudospectral simulations, supporting the contention by Fedioun et al. [9] that numerical error is dominated by the finite-differencing (i.e. truncation) error rather than the aliasing error when performing LES with 2nd order schemes. The result from the pseudospectral simulations were further reinforced by examination of the ratio of numerical dissipation to total dissipation in the finite-volume results, which showed that the Q and 2U schemes introduced less dissipation than the Smagorinsky SGS model. It was also noted that the

82

combination MILES-BCD yielded the best prediction of the energy spectrum, especially for high wavenumbers, due to the minimal amount of dissipation for this combination.

To further highlight the differences in the finite-volume simulations, the asymptotic decay rates were evaluated. The numerical simulations were initialized with a velocity field whose phases are assumed to have adjusted to appropriate values (i.e. a rescaled velocity field). The decay rates predicted with the BCD scheme and the eddy viscosity models overpredicted the experimental value significantly, although the results with the SM model was at the upper limit of values reported in the literature. Although the MILES-BCD combination showed excellent agreement with the experimental data in terms of the energy spectrum, it yielded the worst prediction of decay rate, overpredicting experiments by 45%. The decay coefficients for MILES and the Smagorinsky model with QUICK gave the closest results to the reported experimental data, and suggest that for accurate results in engineering simulations the combination of MILES with QUICK or 2nd order upwind may yield the best results in an overall sense.

Following this, an axisymmetric jet flow following the investigation of Hussein et al. [14] was simulated. It served as an application problem used to verify the results from prior finding of favorable combinations of SGS model and discretization schemes for use in large eddy simulation of turbulent flow. The three combinations examined in the jet flow case were SM-BCD, DSM-BCD and MILES-2U. All of the jet flow cases showed reasonable agreement with experimental data in terms of the spatial decay of centerline velocity. However, the results using MILES-2U were noticeably more accurate than the other two combinations, matching the data almost exactly. Likewise, all three showed

83

good agreement with experiments in terms of radial distributions of mean velocity and Reynolds stresses with MILES-2U slightly outperforming the other two. The relevance of these results is that the findings from prior sections are reinforced.

Taken in their entirety, the results from this study suggest that useful results may be obtained from LES of engineering flows using commonly available discretization schemes (i.e. 2nd order) and SGS models (i.e. eddy-viscosity). Important guiding principles are that the discretization scheme should be non-dispersive, and that the combined effects of the discretization scheme and SGS model should provide a sufficient but not overly large level of dissipation. Satisfying these criteria has been found to result in good prediction of the large-scale flow behavior, including the energy spectrum (except near the cutoff wavenumber), turbulent energy decay, and turbulent mixing dynamics. The four combinations investigated here that most closely meet this requirement are SM-BCD, DSM-BCD, MILES-2U, and MILES-Q. Perhaps surprisingly, it is the latter two, which rely on no explicit SGS model and on strongly upwinded discretization schemes, that yield the best results overall for the test cases considered here.

REFERENCES

[1] "FLUENT$^{\circledR}$ Users Guide version 6.2.16," *FLUENT$^{\circledR}$ INC.*, Lebanon, NH, USA.

[2] T. J. Barth and D. Jesperson, "The Design and Application of Upwind Schemes on Unstructured Meshes," *AIAA Paper*, , no. AIAA-89-0366, 1989, p. 273.

[3] S. Bhushan and Z. U. A. Warsi, "Large eddy simulation of turbulent channel flow using an algebraic model," *International Journal for Numerical Methods in Fluids*, vol. 49, no. 6, 2005, pp. 489–519.

[4] J. P. Boyd, *Chebyshev and Fourier Spectral Methods*, 2nd edition, Dover Publications, Inc, 31 East 2nd Street Mineola, New York 11501, 2000.

[5] C. Canuto, M. Y. Hussaini, A. Quarteroni, and T. A. Zang, *Spectral Methods in Fliud Dynamics*, Springer-Verlag, New York Inc., New York, 1998.

[6] S. Cerutti, C. Meneveau, and O. M. Knio, "Spectral and Hyper eddy viscosity in high-Reynolds-number turbulence," *Journal of Fluid Mechanics*, vol. 421, 2000, pp. 307–338.

[7] G. Comte-Bellot and S. Corrsin, "Simple Eulerian time correlation of full-and-band velocity signals in grid-generated isotropic turbulence," *Journal of Fluid Mechanics*, vol. 48, 1971, p. 273.

[8] P. A. Davidson, *Turbulence An Introduction For Scientist and Engineers*, 1st edition, Oxford University Press, Great Clarendon Street, Oxford ox2 6DP, 2004.

[9] I. Fedioun, N. Lardjane, and I. Gokalp, "Revisiting Numerical Errors in Direct and Large Eddy Simulations of Turbulence: Physical and Spectral Spaces Analysis," *Journal of Computational Physics*, vol. 174, Dec. 2001, pp. 816–551.

[10] C. Fureby and F. F. Grinstein, "Large Eddy simulation of high-Reynolds-number free and wall-bounded flows," *Journal of Computational Physics*, vol. 181, no. 1, 2002, pp. 68–97.

[11] M. Germano, U. Piomelli, P. Moin, and W. H. Cabot, "A Dynamic subgrid-scale eddy viscosity model," *Physics of Fluids*, vol. 3, July 1991, pp. 071760–06.

[12] S. Ghosal, "An Analysis of Numerical Error in Large-Eddy Simulation of Turbulence," *Journal of Computational Physics*, vol. 125, Jan. 1996, pp. 187–206.

[13] J. Gullbrand and F. K. Chow, "The effect of numerical errors and turbulence models in large-eddy simulation of channel flow, with and without explicit filtering," *Journal of Fluid Mechanics*, vol. 495, June 2003, pp. 323–341.

[14] H. J. Hussein, S. P. Capp, and W. K. George, "Velocity measurements in a high-Reynolds-number, momentum-conserving, axisymmetric, turbulent jet," *Journal of Fluid Mechanics*, vol. 258, Jan. 1994, pp. 31–75.

[15] H. S. Kang, S. Chester, and C. Meneveau, "Decaying turbulence in an active-grid-generated flow and comparisons with large-eddy simulation," *Journal of Fluid Mechanics*, vol. 480, no. 480, April 2003, pp. 129 – 160.

[16] A. G. Kravchenko and P. Moin, "On the effects of numerical errors in large eddy simulation of turbulent flow," *Journal of Computational Physics*, vol. 131, 1997, pp. 310–322.

[17] B. P. Leonard, "A Stable and Accurate Convective Modelling Procedure Based on Quadratic Upstream Interpolation," *Computer Methods in Applied Mechanics and Engineering*, vol. 19, 1979, pp. 59–98.

[18] H. Makita, "Realization of large-scale turbulence field in a small wind tunnel," *Fluid Dynamics Res.*, vol. 8, 1991, pp. 53–64.

[19] M. S. Mohamed and J. C. LaRue, "The Decay Power Law in Grid-Generated Turbulence," *Journal of Fluid Mechanics*, 1990.

[20] L. Mydlarski and Z. Warhaft, "On the onset of high-Reynolds-number grid-generated wind tunnel turbulence," *Journal of Fluid Mechanics*, vol. 320, 1996, pp. 331–368.

[21] L. Mydlarski and Z. Warhaft, "Passive scalar statistics in high Peclet number grid turbulence," *Journal of Fluid Mechanics*, vol. 358, 1998, pp. 135–175.

[22] N. Park and K. Mahesh, "Analysis of numerical errors in large eddy simulation using statistical closure theory," *Journal of Computational Physics*, vol. 222, no. 1, 2007, pp. 194–216.

[23] N. Park, J. Y. Yoo, and H. Choi, "Discretization errors in large eddy simulation: on the suitability of centered and upwind-biased compact difference schemes," *Journal of Computational Physics*, vol. 198, 2004.

[24] S. B. Pope, *Turbulent Flows*, 1st edition, Cambridge University Press, The Edinburgh Building, Cambridge, CB2 2RU, UK, 2000.

[25] S. B. Pope, "Ten questions concerning the large-eddy simulation of turbulent flows," *New Journal of Physics*, vol. 6, Mar 2004, p. 35.

[26] R. S. Rogallo, "Numerical Experiments in Homogeneous Turbulence," *NASA TM 73202*, 1981.

[27] F. Sarghini, U. Piomelli, and E. Balaras, "Scale-similar models for large-eddy simulations," *Physics of Fluids*, vol. 11, no. 6, June 1999, pp. 1596–1607.

[28] J. Smagorinsky, "General circulation experiment with the primitive equations," *Monthly Weather Review*, vol. 91, Mar 1963, pp. 99–194.

[29] G. D. Stefano and O. V. Vasilyev, "Sharp cutoff versus smooth filtering in large eddy simulation," *Physics of Fluids*, vol. 14, no. 1, Jan. 2002, pp. 362–369.

[30] D. K. Walters and S. Bhushan, "A note on spectral energy transfer for multiscale eddy viscosity models in large-eddy simulation," *Physics of Fluids*, vol. 17, Nov. 2005, pp. 118102–118106.

[31] D. K. Walters and S. Bhushan, "Specification of Time-Dependent Inlet Boundary Conditions for LES, VLES, and DES of Turbulent Flow," *AIAA*, , no. AIAA-2005-1284, 2005.

[32] R. F. Warming and R. M. Beam, "Upwind Second-Order Difference Schemes and Application in Aerodynamics Flows," *AIAA Journal*, vol. 14, no. 9, 1976, pp. 1241–1249.

APPENDIX

FIGURE DETAILS

Figure 6.7: Comparison of centerline velocity variation with distance from the jet exit for experimental data (SHW Data Hussein et al. 1994) and large eddy simulation data for a combination of MILES-2U, DSM-BCD and SM-BCD.

Figure 6.8: Comparison of mean velocity profile for experimental data (FHW, SHW and LDA Data Hussein et al. 1994) and large eddy simulation data for a combination of MILES-2U, DSM-BCD and SM-BCD at downstream distance 50D.

Figure 6.9: Comparison of mean velocity profile for experimental data (FHW, SHW and LDA Data Hussein et al. 1994) and large eddy simulation data for a combination of MILES-2U, DSM-BCD and SM-BCD at downstream distance 70D.

Figure 6.10: Comparison of mean velocity profile for experimental data (FHW, SHW and LDA Data Hussein et al. 1994) and large eddy simulation data for a combination of MILES-2U, DSM-BCD and SM-BCD at downstream distance 90D.

Figure 6.11: Comparison of axial component of turbulent kinetic energy for experimental data (LDA and FHW Data Hussein et al. 1994) and large eddy simulation data for a combination of MILES-2U, DSM-BCD and SM-BCD at downstream distance 50D.

Figure 6.12: Comparison of axial component of turbulent kinetic energy for experimental data (LDA and FHW Data Hussein et al. 1994) and large eddy simulation data for a combination of MILES-2U, DSM-BCD and SM-BCD at downstream distance 70D.

Figure 6.13: Comparison of axial component of turbulent kinetic energy for experimental data (LDA and FHW Data Hussein et al. 1994) and large eddy simulation data for a combination of MILES-2U, DSM-BCD and SM-BCD at downstream distance 90D.